

CMS Draft Analysis Note

The content of this note is intended for CMS internal use and distribution only

2012/12/03

Head Id: 159874

Archive Id: 159892M

Archive Date: 2012/12/03

Archive Tag: trunk

Measurement of the Muon Charge Asymmetry in Inclusive $pp \rightarrow W(\mu\nu) + X$ Production at $\sqrt{s} = 7$ TeV

A. Khukhunaishvili¹, L. Gibbons¹, J. Han², A. Bodek², J. Butler³, D. Green³, S. Kwan³,
J.C. Yun³, S. Ghosh⁴, G. Majumder⁴, S. Guragain⁵, N. Parashar⁵, S. Malik⁶, Y. Onel⁷,
J. Nachtman⁷, and P. Tan⁷

¹ Cornell University, Ithaca, USA

² Rochester University, Rochester, USA

³ Fermilab, Batavia, USA

⁴ TIFR, India

⁵ Purdue University - Calumet, USA

⁶ University of Nebraska-Lincoln, USA

⁷ University of Iowa, USA

Abstract

We present an update of the muon charge asymmetry in pp collisions at $\sqrt{s} = 7$ TeV using a dataset corresponding to an integrated luminosity of $2.xx \text{ fb}^{-1}$ collected with the Compact Muon Solenoid (CMS) Detector at the LHC.

This box is only visible in draft mode. Please make sure the values below make sense.

PDFAuthor:	All
PDFTitle:	Measurement of the Muon Charge Asymmetry in Inclusive $pp \rightarrow W(\mu\nu) + X$ Production at $\sqrt{s} = 7$ TeV
PDFSubject:	CMS
PDFKeywords:	CMS, physics, software, computing

Please also verify that the abstract does not use any user defined symbols

1 Introduction

In pp collisions, W bosons are produced primarily via the processes $u\bar{d} \rightarrow W^+$ and $d\bar{u} \rightarrow W^-$. The first quark is a valence quark from one of the protons, and the second one is a sea antiquark from the other proton. Due to the presence of two valence u quarks in the proton, there is an overall excess of W^+ over W^- bosons. The inclusive ratio of cross sections for W^+ and W^- boson production at the Large Hadron Collider (LHC) was measured to be 1.43 ± 0.05 by the Compact Muon Solenoid (CMS) experiment [1] and is in agreement with predictions of the Standard Model (SM) based on various parton distribution functions (PDFs) [2, 3]. Measurement of this production asymmetry between W^+ and W^- bosons as a function of boson rapidity can provide new insights on the u/d ratio and the sea antiquark densities in the ranges of the Björken parameter x [4] probed in pp collisions at $\sqrt{s} = 7$ TeV. However, due to the presence of neutrinos in leptonic W decays, the boson rapidity is not directly accessible. The experimentally accessible quantity is the lepton charge asymmetry, defined to be

$$\mathcal{A}(\eta) = \frac{d\sigma/d\eta(W^+ \rightarrow \ell^+\nu) - d\sigma/d\eta(W^- \rightarrow \ell^-\bar{\nu})}{d\sigma/d\eta(W^+ \rightarrow \ell^+\nu) + d\sigma/d\eta(W^- \rightarrow \ell^-\bar{\nu})}$$

where ℓ is the daughter charged lepton, η is the charged lepton pseudorapidity in the CMS lab frame ($\eta = -\ln[\tan(\frac{\theta}{2})]$ where θ is the polar angle), and $d\sigma/d\eta$ is the differential cross section for charged leptons from W boson decays. The lepton charge asymmetry can be used to test SM predictions with high precision.

The lepton charge asymmetry and the W charge asymmetry have been studied in $p\bar{p}$ collisions by both the CDF and D0 experiments at the Fermilab Tevatron Collider [5, 6]. A high precision measurement of this asymmetry at the LHC can contribute to the improvement of the knowledge of PDFs. ATLAS, CMS, and LHCb experiments have reported measurements of the lepton charge asymmetry at the LHC recently using the data collected during 2010 LHC runs [7–9]. Latest updates on the lepton charge asymmetry using CMS data are reported here [10] [11], which use 840 pb^{-1} and 234 pb^{-1} for electron and muon channel respectively. For the muon channel, more details can be found in internal analysis notes [12] [13] [14].

In this note, we are updating the muon charge asymmetry with a much larger dataset than previous results. The analysis twiki page is at,

<https://twiki.cern.ch/twiki/bin/viewauth/CMS/ChargeAsymmetry2012>.

2 Datasets

Table and Table shows the MC simulation and datasets used in this analysis.

Table 1: MC simulation used in this analysis.

fill me later

Table 2: Datasets used in this analysis.

fill me later

We primarily use POWHEG [15] MC simulation interfaced with CT10 PDF model [3] except that for QCD multijet background we use Pythia [16] event generator with CTEQ6L [17] PDF models. The normalization cross sections are the recommended ones as shown in this twiki page,

<https://twiki.cern.ch/twiki/bin/view/CMS/StandardModelCrossSections>

30 We use the single muon primary dataset, “/SingleMu/Run2011A-08Nov2011-v1/AOD”. The
31 good runs/luminosity sections are selected based on json file,

Cert_160404-180252_7TeV_ReRecoNov08_Collisions11_JSON_v2.txt

We utilize a single muon trigger path,

HLT_IsoMu24(15)*.

32 During part of 2011 data-taking period, this trigger path has been prescaled for part of the
33 luminosity sections. We explicitly exclude these luminosity sections. The total luminosity is
34 about xx.

35 Several event filters are applied,

- 36 • Beam halo and beam background remove, “FilterOutScraping”.
- 37 • At least one good offline primary vertex, “GoodVertexFilter”.
- 38 • HBHENoiseFilter, “HBHENoiseFilter”.

39 only events passing these filters are used.

40 3 Event Selection

41 The experimental signature of inclusive W boson production is a high- p_T lepton accompa-
42 nied by a large Missing Transverse Energy (ME_T). The CMS detector is designed to have very
43 high efficiency to trigger on high- p_T muons. Other processes such as QCD multi-jet produc-
44 tion (QCD background), Drell-Yan production, $W \rightarrow \tau\nu$ (EWK background), and $t\bar{t}$ can fake
45 signal candidates.

46 3.1 Triggers

47 As shown in Table 2, depending on the run period different trigger paths are used in this
48 measurements. However, in MC only the HLT_Mu9 trigger path is considered.

49 3.2 Candidate Selection

The muon candidate are identified using “tight” criteria, as described here,

<https://twiki.cern.ch/twiki/bin/view/CMSPublic/SWGuideMuonId#The2011Data>

50 For convenience, the detail of the selections are listed as below,

- 51 • muons are within pseudorapidity coverage, $\eta < 2.4$.
- 52 • muon were identified as both a “GlobalMuon” and a “TrackerMuon” candidate,
- 53 • normalized global track fitting $\chi^2 < 10$,

- 54 • at least 9 silicon tracker layers,
- 55 • at least 1 muon chamber hit included in the global muon track fit,
- 56 • at least 2 segments in muon stations,
- 57 • at least 1 pixel hit included in the inner silicon track fit,
- 58 • Closest approach of the tracker-track with respecting to leading primary vertex is
- 59 less than 2 mm,

60 We further require that the muons have to pass the “loose” isolation criteria, which implies the
61 relative track-based isolation < 0.1 . We infer muons passing above criteria as “isolated loose”
62 muons.

63 The “isolated loose” muon candidate passing above selection criteria with largest p_T is selected
64 as the $W \rightarrow \mu\nu$ signal candidate, and it is further required to pass,

- 65 • $p_T > 25$ GeV,
- 66 • match to a HLT trigger candidate used to select the data set with $\Delta R(\mu, HLT) < 0.1$.

67 The Drell-Yan background contribution is reduced by rejecting events that contain at least a
68 second “isolated loose” muon with $p_T > 15$ GeV. By inverting the “Drell-Yan veto” selection,
69 we defined a “Drell-Yan control region”.

After above event selections, all events are divided into different muon pseudorapidity bins to measure the muon charge asymmetry as a function of muon pseudorapidity. The bins we use are based on the absolute value of the muon pseudorapidity, and the exact binning is as follows:

$$[0, 0.2, 0.4, 0.6, 0.8, 1.0, 1.2, 1.4, 1.6, 1.85, 2.1, 2.4]$$

70 After event selections described above, the QCD background is still significant. The Drell-Yan
71 background is the dominant EWK background. The dominant contribution of the Drell-Yan
72 background is where one of the daughter muons is outside the “Drell-Yan” veto region. In the
73 forward region, it is estimated to be about 10% of the signal yield. The $W \rightarrow \tau\nu$ background
74 is about 3-4% of the signal yield, and the ratio to $W \rightarrow \mu\nu$ signal has little pseudorapidity
75 dependence. The $t\bar{t}$ background is only about 0.5% of the expected signal yield. The cosmic
76 muon contamination in our data sample is negligible, according the previous studies.

77 3.3 Pile-up (PU) Reweighting

78 The PU is significant in the data sample, and the average number of reconstructed vertices is
79 about 8-9. The MC simulation are reweighted to match the number of reconstructed vertices in
80 data, according a recipe described here (“3-D PU reweight”).

81 3.4 Kinematic Distributions

82 Figure 1 shows the p_T , η , E_T^{miss} , and M_T distributions for signal muon candidates within $yy <$
83 $\eta < xx$.

84 4 Muon Efficiency

The efficiency is parameterized in the tracking (tracking), the global muon reconstruction (global), the muon identification (ID), the isolation (iso), and HLT trigger efficiency (HLT),

$$\epsilon = \epsilon_{\text{tracking}} \times \epsilon_{\text{global}} \times \epsilon_{\text{ID}} \times \epsilon_{\text{iso}} \times \epsilon_{\text{HLT}} \quad (1)$$

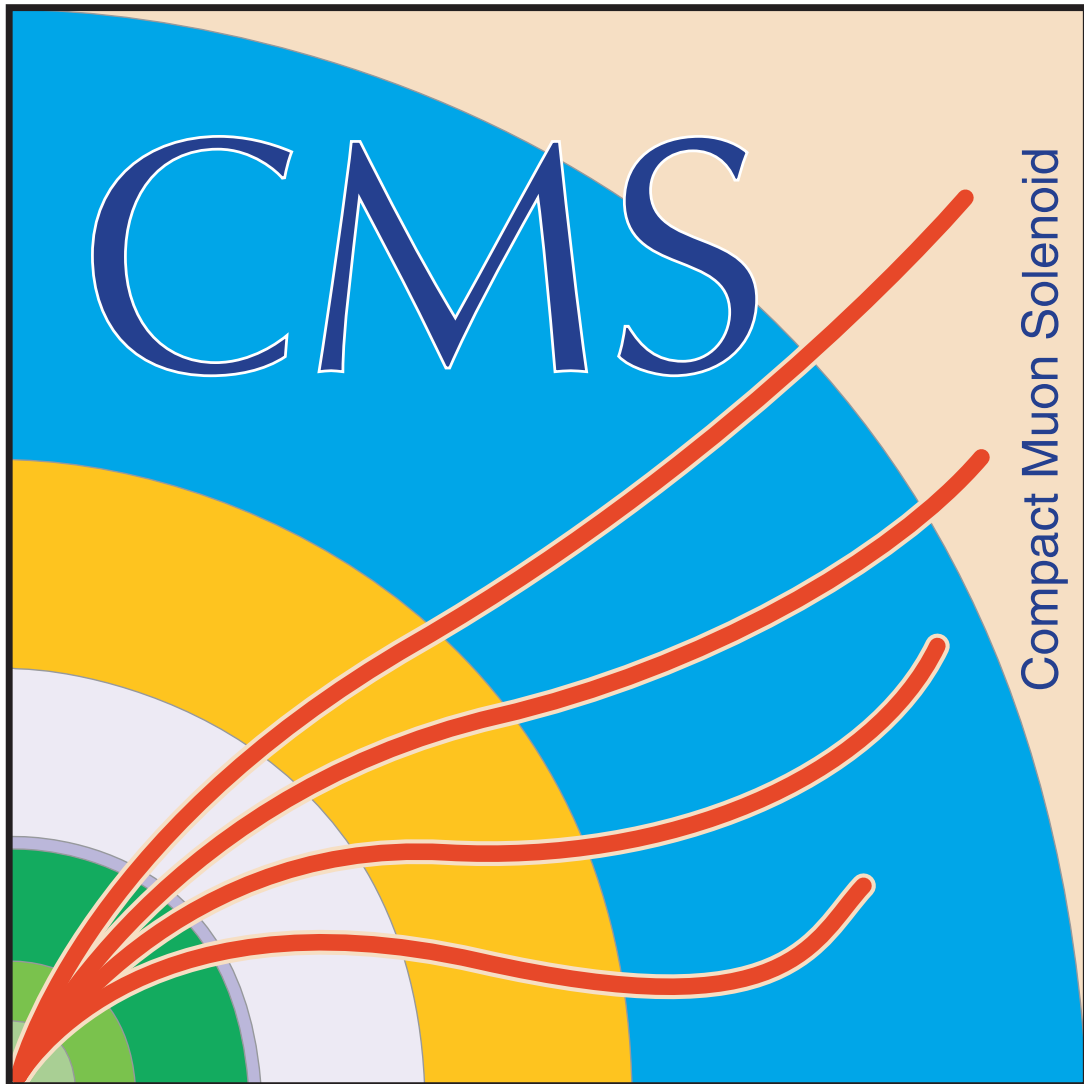


Figure 1: The p_T , η , E_T^{miss} , and m_T distributions for signal muon candidates within $yy < \eta < xx$. MC simulation is normalized to data luminosity.

85 These efficiencies are estimated using the tag and probe method (T&P) in Z sample. A binned
 86 likelihood fit is performed over the Z mass spectrum to estimate the signal and background
 87 contributions, and a mass window of [60, 120] GeV has been used in the fit. We only use events
 88 in the tight mass window, $80 < M_{\mu\mu} < 100 \text{ GeV}/c^2$, to calculate the efficiencies. The tagged leg
 89 is required to have the tight muon selection defined in CMS with $p_T > 25 \text{ GeV}/c$ including the
 90 trigger object matching to clean up the sample and probe leg is used to measure the efficiency.
 91 The data and MC has the different pile-up scenario, so the pile-up weighting is applied into
 92 MC to the same pile-up distribution with data.

93 A general track is used as a probe to measure the global muon reconstruction efficiency. To
 94 measure the muon identify efficiency, we use a global muon as a probe and require it to pass
 95 the “tight” muon selection criteria described in Section 3.2. The isolation criteria used in this
 96 analysis is the “loose” relative track-based isolation ($E_{iso}^{trk}/p_T < 0.1$), and a “tight” global muon
 97 is used as a probe to measure it. We determine the trigger efficiency using a “isolated tight”
 98 muon as a probe. The tracking efficiency for muons is found to be almost 100%.

99 All efficiencies are determined as a function of the pseudo-rapidity (η) and p_T of muon object.
 100 The efficiencies are obtained from T&P method using $xx \text{ fb}^{-1}$ of the integrated luminosity.
 101 The total efficiency is calculated by multiplying the efficiencies ($\epsilon_{global} \times \epsilon_{ID} \times \epsilon_{iso} \times \epsilon_{HLT}$). We
 102 measure the efficiency for μ^+ and μ^- , respectively, to check the charge dependence. Figure 2-4
 summarize the results.

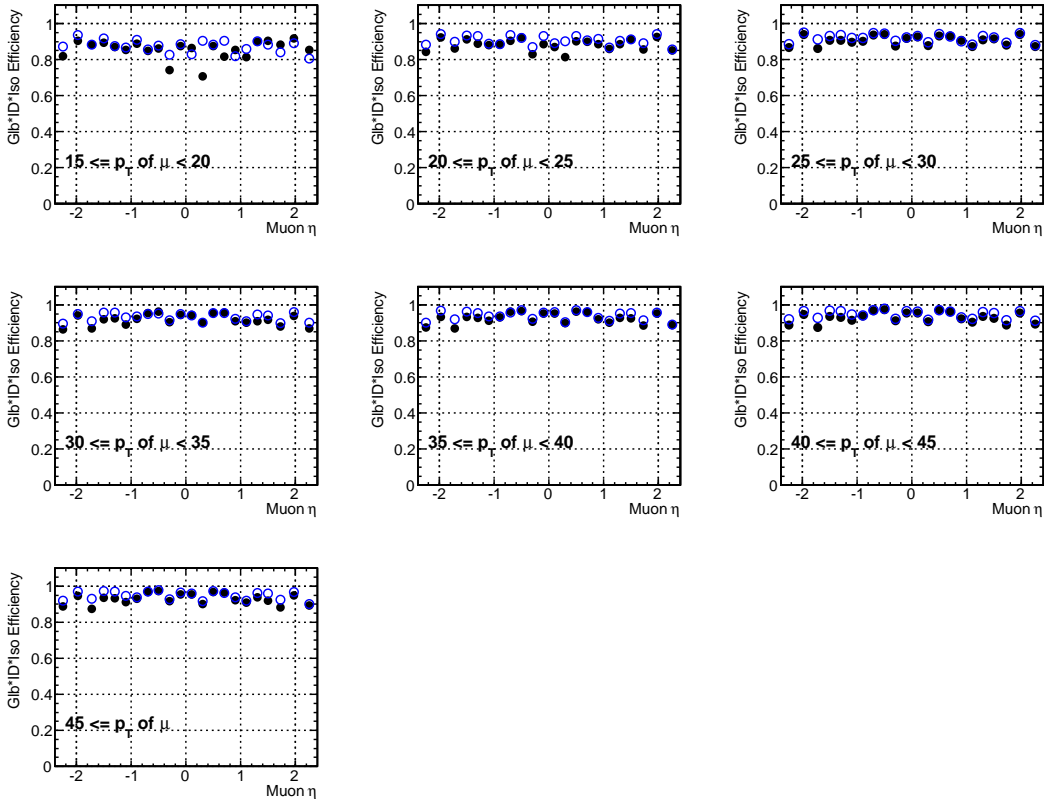


Figure 2: The efficiency for Global×ID×Isolation in η and p_T of μ^- . The black points are data and the blue circles are MC.

103

104 The efficiency scale factor of the data to MC is applied into MC to match the signal shape

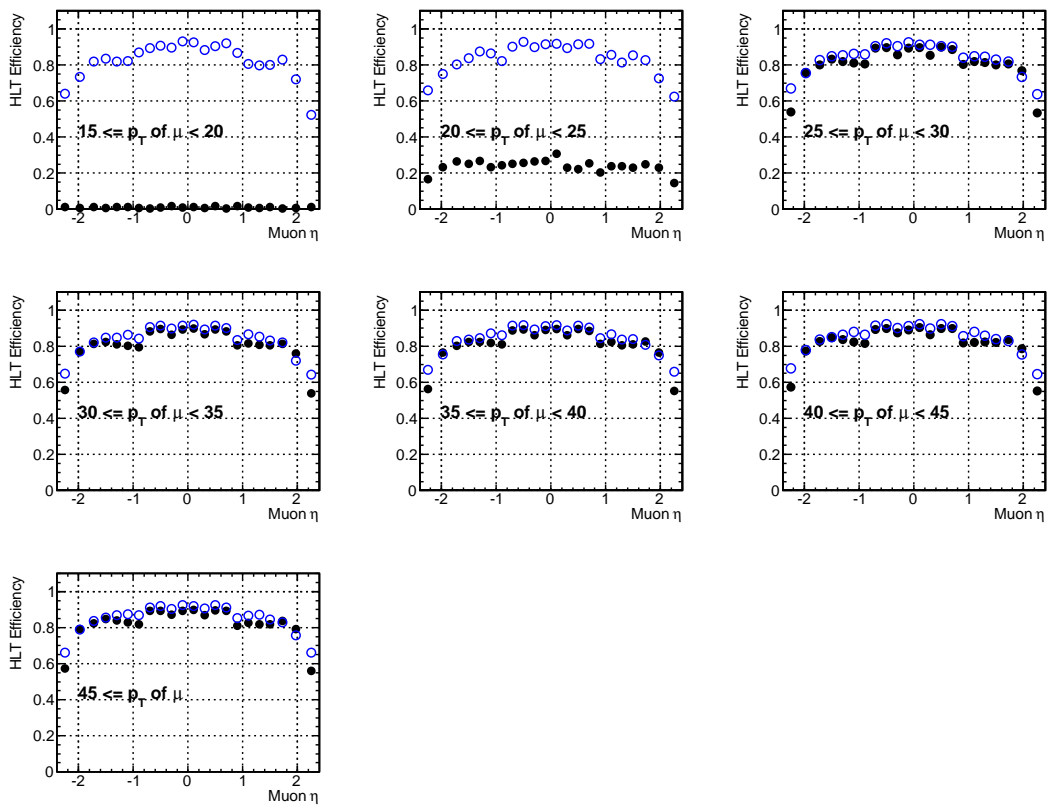


Figure 3: The efficiency for $HLT_IsoMu15(24)^*$ triggers in η and p_T of μ^- used in this analysis. The black points are data and the blue circles are MC.

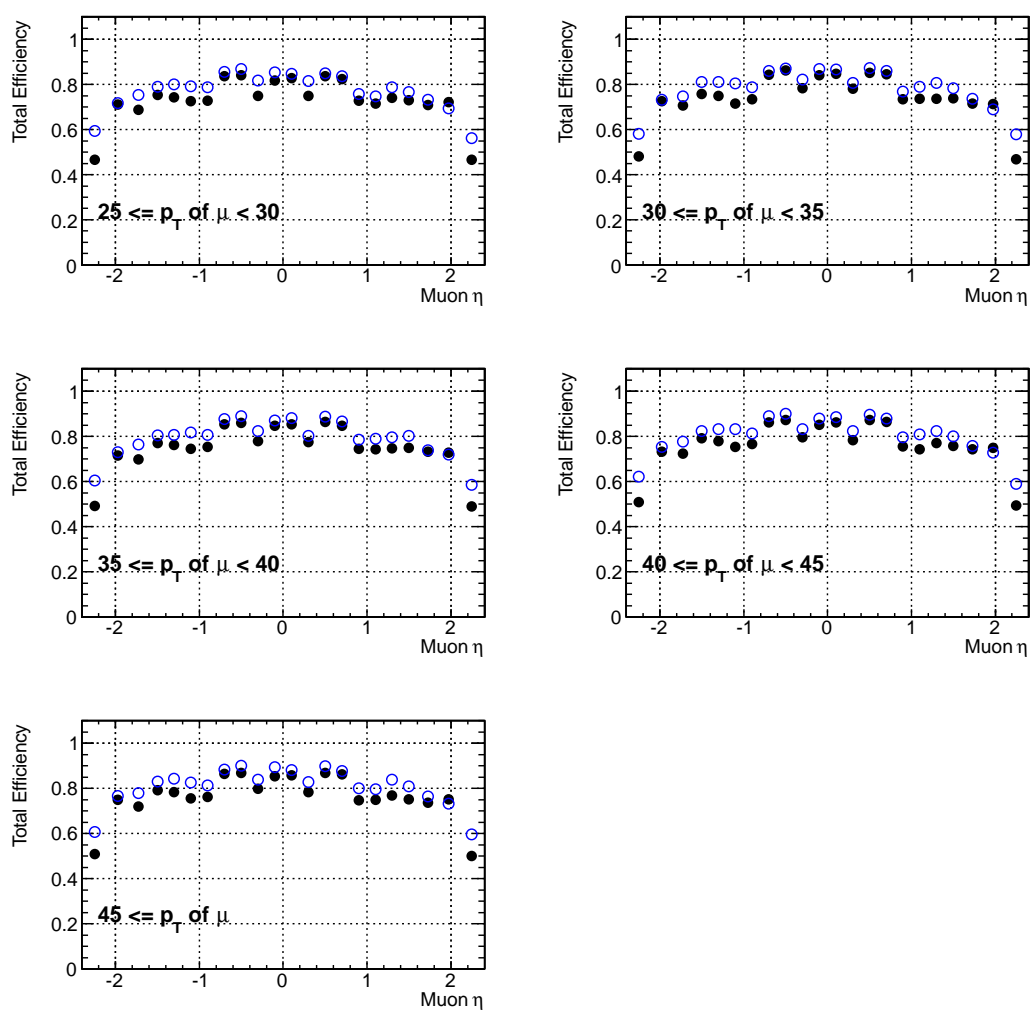


Figure 4: The total efficiency for μ^- as a function of muon η and p_T .

105 between data and MC. (It corrects the background normalization and MET shape for the back-
 106 ground extraction.) The efficiency and its scale factor of data to MC for the global reconstruction, ID, and isolation cut in $p_T > 15$ GeV/c are shown in Figure 5 and 6.

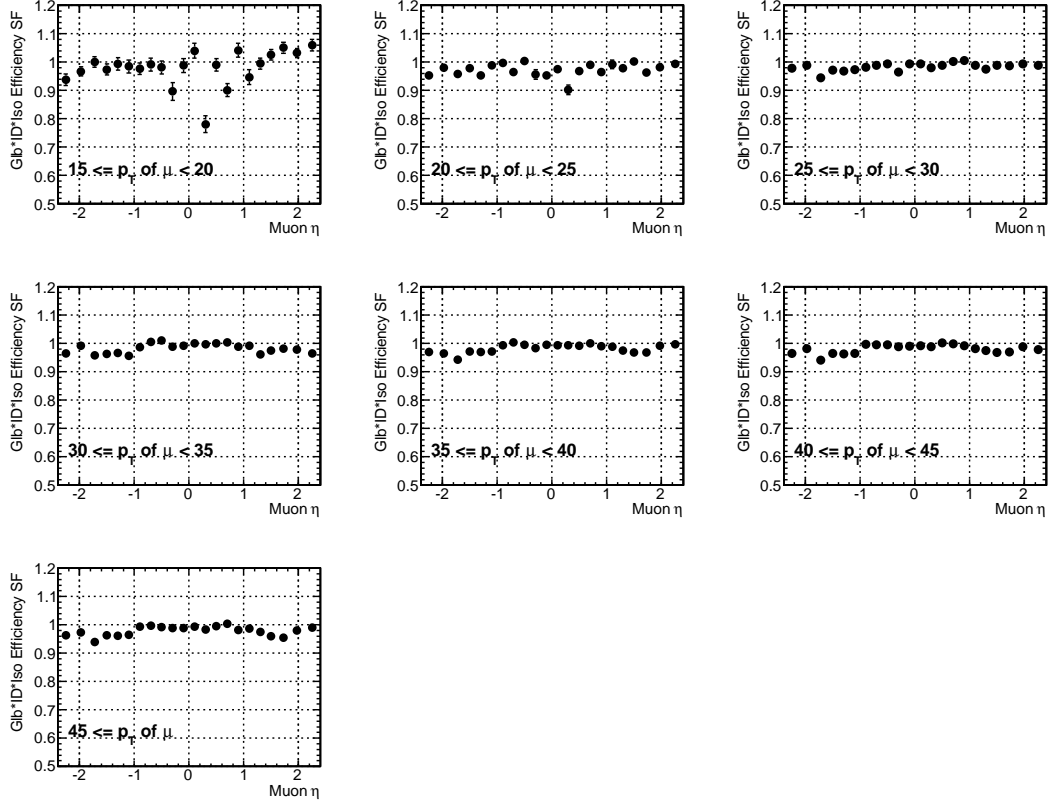


Figure 5: The efficiency scale factor of data to MC for Global \times ID \times Isolation in η and p_T of μ^- .

107

108 The lepton charge asymmetry is sensitive to the charge dependence of the efficiency, so we
 109 measure the efficiency ratio of μ^+ to μ^- as a function of $|\eta|$. Figure 7 shows the efficiency ratio
 110 of μ^+ to μ^- in $|\eta|$ and p_T . The efficiency ratio is fitted using $f(p_T) = p_0$ in $p_T > 25$ GeV/c
 111 where is p_T range for the lepton charge asymmetry. The fit results are summarized in Table
 112 3. We confirmed the fit result measuring the inclusive efficiency in $p_T > 25$ GeV/c and both
 113 values are close to be identical. In the forward region, the efficiency shows a minor charge
 114 dependence.

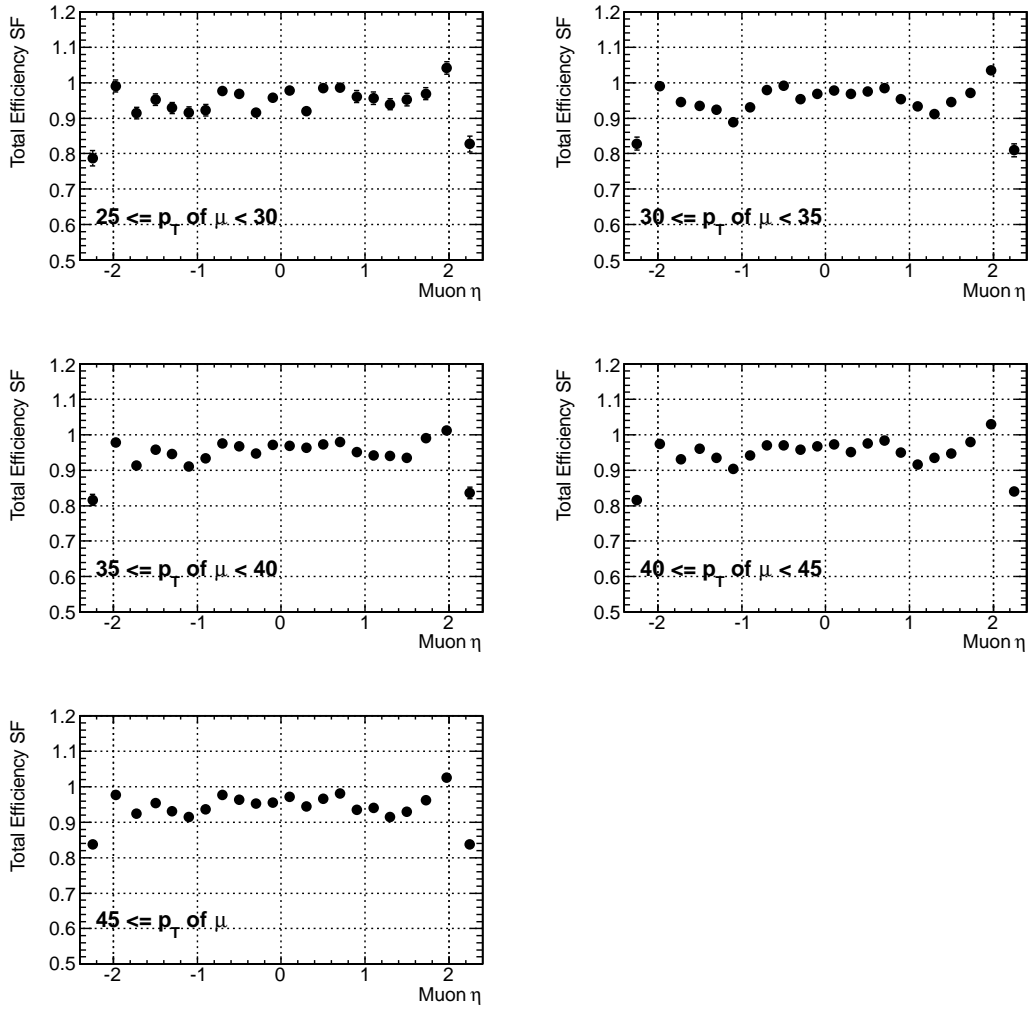


Figure 6: The total efficiency scale factor of data to MC in η and p_T of μ^- . The plot shows the scale factor for the lepton charge asymmetry ($p_T > 25 \text{ GeV}/c$).

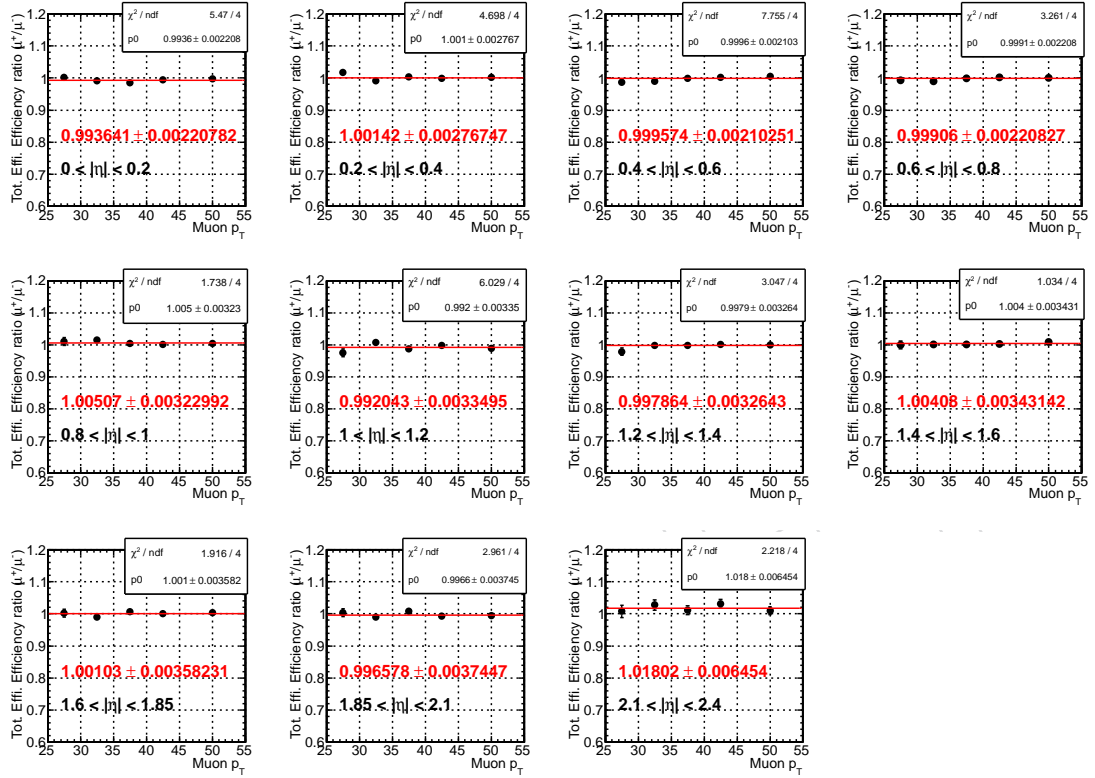


Figure 7: The total efficiency ratio of μ^+ to μ^- in $|\eta|$. The efficiency ratio is fitted by the constant function in $p_T > 25$ GeV/c. The fit result is used to assign the systematic uncertainty of the efficiency.

Table 3: The fit result of the efficiency ratio of μ^+ to μ^- in $|\eta|$. The fit result is determined in $p_T > 25$ GeV/c.

η bin	$\epsilon(\mu)$ Ratio of μ^+ to μ^-
$0.00 < \eta < 0.20$	0.9936 ± 0.0022
$0.20 < \eta < 0.40$	1.0014 ± 0.0028
$0.40 < \eta < 0.60$	0.9996 ± 0.0021
$0.60 < \eta < 0.80$	0.9991 ± 0.0022
$0.80 < \eta < 1.00$	1.0051 ± 0.0032
$1.00 < \eta < 1.20$	0.9920 ± 0.0033
$1.20 < \eta < 1.40$	0.9979 ± 0.0033
$1.40 < \eta < 1.60$	1.0041 ± 0.0034
$1.60 < \eta < 1.85$	1.0010 ± 0.0036
$1.85 < \eta < 2.10$	0.9966 ± 0.0037
$2.10 < \eta < 2.40$	1.0180 ± 0.0065

5 Muon Momentum Scale and Misalignment Correction

A muon momentum correction is applied to compensate for misalignment of the CMS detector. The primary cause of bias in the reconstructed momentum is the misalignment of the tracker. The tracker geometry is not well modeled in data. It is not well modeled in MC either. Therefore, the reconstructed momenta are biased in both data as well as in MC. The misalignments in data and MC are different.

We extract the corrections for both data and MC samples in the same way. The sample used for the study (the Drell-Yan dimuon sample) corresponds to 2.1 fb^{-1} of integrated luminosity of data collected during the early 2011 runs. The corrections to the muon momentum in both data and MC are extracted using the average of $1/p_T$ (i.e. $\langle 1/p_T \rangle$) spectra of muons from Z decays in the bins of muon charge (Q), θ , and ϕ , as described in CMS note AN-12-062. We extract correction factors for positive and negative muons. By taking the sum and difference of the correction factors for positive and negative muons we extract additive and multiplicative corrections to $1/p_T$. The additive corrections comes from a misalignment, and a multiplicative correction comes from an error in the integral of B^*dL . On top of $\langle 1/p_T \rangle$ correction, we extract the additional correction factors using the average of Z mass, $\langle M_{\mu\mu}^Z \rangle$, in η and ϕ bin. The tagged leg of two muons determines η and ϕ bin of μ^+ or μ^- . The other leg can be anywhere in η and ϕ , so the effect averages out. The Z mass is less sensitive to the efficiencies, background, and modeling of kinematic distributions. Therefore, the additional correction using Z mass reduces the systematic uncertainty of the correction. This additional correction from Z mass is also propagated into $\langle 1/p_T \rangle$ correction at the end. The improvement of the muon momentum scale using Z mass is described in CMS note AN-12-298.

For the lepton charge asymmetry, we extract the correction using the data in CMSSW 44x release. The detector alignment in η is improved in 44x release, so the correction in 44x is smaller than 42x. To reduce the correlation among the bins, the muon momentum correction is extracted using the same η binning with the lepton charge asymmetry analysis.

As a check on the procedure, we compared kinematic distributions for the data and MC before and after the momentum corrections. Before the momentum corrections, the forward-backward asymmetry of dimuons had unphysical wiggles that can only originate from a bias in reconstruction of positive and negative muons. The ϕ distribution of Z bosons in the Collins-Soper Frame also showed unphysical features that indicated a bias in reconstruction of pos-

146 itive and negative muons. The Z mass was found to be a function of ϕ and η and sign of
 147 the muon. None of these distributions were used in the extraction of the momentum correc-
 148 tions. After the momentum corrections, all of the unphysical features are removed and the
 149 average Z mass is independent of ϕ and at the correct mass value. The small η and muon sign
 150 dependence of the average Z mass is now in good agreement with expectation (the small η de-
 151 pendence originates from the P_T cuts on the sample, and the small sign dependence originates
 152 from the forward-backward electroweak asymmetry). After the application of the momentum
 153 corrections, the mass of the Z peak (determined from a bit to a narrow mass window) was
 154 found to be different from the expected mass by only $0.03\% \pm 0.01\%$ for the data and $0.00\% \pm$
 155 0.01% for the MC. We correct for the small shift in the data by the application of an addition
 156 overall scale correction.

157 During the study, we found that 2011A and 2011B data set has slightly different bias in ϕ shown
 158 in 8. Therefore, we extract the muon momentum correction for 2011A and 2011B, respectively,
 159 and apply into the data. (MC doesn't have any run dependence in the muon momentum cor-
 160 rection.)

161 After the application of the momentum corrections to the data and MC we find that the Z line
 162 shape shows a good agreement between data and MC in 44x release. Figure 9 and 10 show
 163 the reference plots after the correction in 2011A data set. These plots are used to check the
 164 procedure of the correction. After the correction, the data and MC show a good agreement
 165 each other and all of the muon momentum bias is removed.

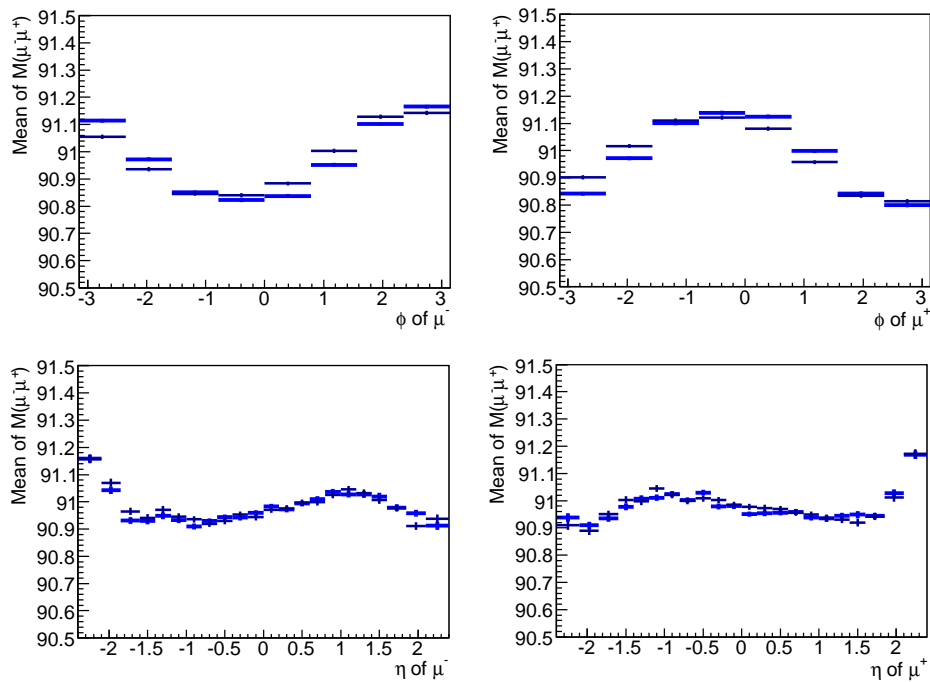


Figure 8: The Z mass profile in muon ϕ and η in 2011A and 2011B data. The black line shows the Z mass profile of 2011A data and the blue line shows 2011B data. The ϕ dependence is not same between 2011A and 2011B data even though the η dependence is close each other.

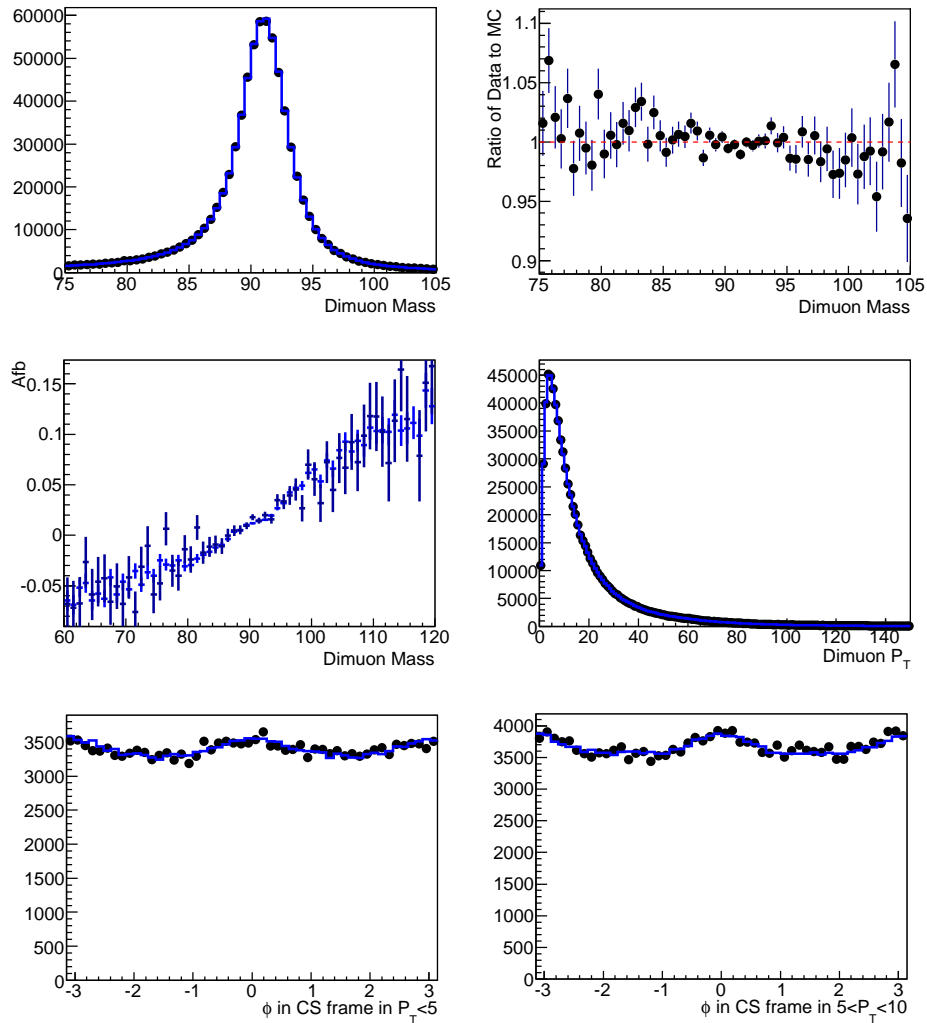


Figure 9: The first reference plot of the muon momentum correction after the correction in 2011A data : Z mass, A_{FB} , $Z P_T$, and ϕ in Collins-soper frame in low $Z P_T$. The plots in the first row show the dimuon distribution in data (black) and MC (blue) and its ratio. The plot in the left side of the second row shows the forward-backward asymmetry and the plot in the right side shows $Z P_T$ distribution. The $Z P_T$ distribution in MC is tuned to match the data. The plots in the bottom show ϕ distribution in Collins-soper frame in $Z P_T < 5$ (left) , $5 < Z P_T < 10$ GeV/c (right). The black points corresponds to data and the blue to MC.

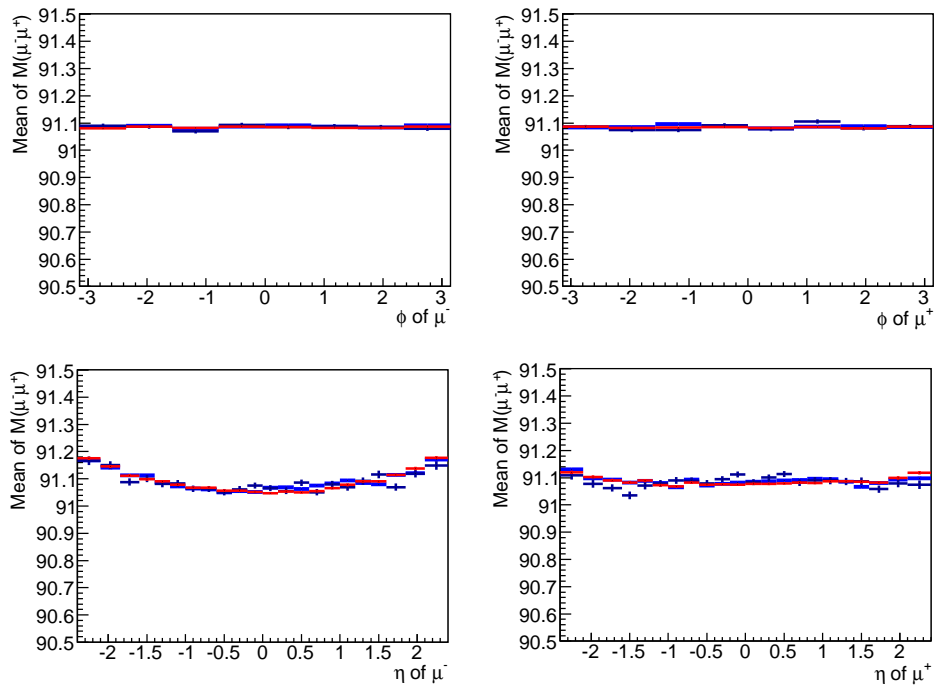


Figure 10: The second reference plot of the muon momentum correction after correction in 2011A data: Z mass profile in muon ϕ and η . The plots in top show the Z mass profile in ϕ of μ^- (left) and μ^+ (right) and the plots in bottom show the Z mass profile in η of μ^- (left) and μ^+ (right). The Z mass corresponds to the average of Z mass in the range of $86.5 < M(\mu\mu) < 96.5$ GeV/c^2 . The black points are data, the blue points are MC, and the red points are the generated level after QED radiation which is used as the reference point.

6 Background Study and Signal Estimation

6.1 Overview of Method

We measure the W muon charge asymmetry in 11 bins of muon pseudorapidity:

$$[0, 0.2, 0.4, 0.6, 0.8, 1.0, 1.2, 1.4, 1.6, 1.85, 2.1, 2.4]$$

To extract the signal yield and calculate the asymmetry we perform the binned maximum likelihood fit of missing transverse energy distribution in data with Monte-Carlo simulation. In each pseudorapidity bin the fit is performed for each muon charge simultaneously floating the following three parameters:

- Number of W^+ events: N_+
- Number of W^- events: N_-
- Scale factor for QCD yield: α_{QCD} ,

while the EWK and $t\bar{t}$ backgrounds are normalized to the integrated luminosity. The background normalization is corrected for different muon efficiencies in data and simulation by re-weighting each event by $\epsilon_{data}/\epsilon_{mc}(p_T, \eta)$. Then we calculate the "raw" asymmetry and its error in each pseudorapidity bin with the following equations:

$$A_0 = \frac{N_+ - N_-}{N_+ + N_-} \quad (2)$$

$$\delta A_0 = \sqrt{f_+^2 \delta N_+^2 + f_-^2 \delta N_-^2 + 2f_+ f_- cov(N_+, N_-)}, \quad (3)$$

where $f_{\pm} = \pm 2N_{\mp}/(N_+ + N_-)^2$. Non-zero correlation between N_+ and N_- is induced by the common QCD scale factor for each W sign, such that $\rho(N_+, N_-) = \rho(N_+, \alpha_{QCD}) \times \rho(N_-, \alpha_{QCD})$.

At the end we correct the measured raw asymmetry above for the different efficiencies for positive and negative muons:

$$A = A_0 - \frac{1 - A_0^2}{2} \left(\frac{\epsilon^+}{\epsilon^-} - 1 \right). \quad (4)$$

6.2 Tuning of Missing transverse energy

We start from the Particle Flow based missing transverse energy and apply several corrections to it. First we correct the measured MET for muon scale by adding the muon transverse momentum correction vectorially to $E_T^{\vec{m}iss}$ in both, data and Monte-Carlo. Then we remove the transverse momentum ϕ modulation in data and Monte-Carlo separately. We derive this correction using our Drell-Yan control sample. At the end, we apply the hadronic recoil technique to correct the recoil response and resolution in Monte-Carlo to match with data. In the following subsections we describe these corrections and test them in Drell-Yan control sample.

6.2.1 Recoil definition

The recoil is defined as a vector sum of all particle flow candidate transverse momenta, excluding muons which come from the boson decay. In Drell-Yan sample it can be written as:

$$\vec{u} = -E_T^{\vec{m}iss} - \vec{q}_T \quad (5)$$

where \vec{q}_T is the transverse momentum of di-muon system, while in W events it is written as:

$$\vec{u} = -E_T^{\text{miss}} - \vec{p}_T^\mu \quad (6)$$

190 We then define the parallel and perpendicular component of this vector relative to boson di-
 191 rection as u_{\parallel} and u_{\perp} respectively. In order to define boson q_T and direction, we use the re-
 192 constructed muon whenever possible. So, in Drell-Yan control sample, we define the bo-
 193 son momentum as that of reconstructed di-muon system, in W signal events we define it as
 194 $\vec{q}_W = \vec{p}_\mu^{\text{reco}} + \vec{p}_\nu^{\text{gen}}$, while in $W \rightarrow \tau\nu$ events we use the generated W momentum.

195 For Drell-Yan Monte-Carlo in signal region (i.e. events pass DY-veto), we split the events into
 196 two categories based on the direction of second generated muon.

- 197 • If the generated second muon falls within the tracker fiducial (failing some of muon
 198 quality criteria, e.g. isolation), the MET distribution looks like in zero-true-MET
 199 sample, so we define the recoil and recoil axes like in Drell-Yan control sample, using
 200 generated muon instead of the reconstructed one.
- 201 • When the second muon falls outside of tracker coverage, the muon behaves like
 202 neutrino and the recoil and recoil axes is defined as in W signal, replacing neutrino
 203 with generated muon.

204 6.2.2 Φ modulation correction

We derive the correction for ϕ modulation by looking at the average perpendicular recoil as
 a function of boson ϕ for different number of reconstructed vertices in both data and MC. We
 first correct the E_T^{miss} for muon momentum scale in both data and MC. Then we look at the
 average u_{\parallel} profile as a function of boson q_T and fit it with the following function:

$$-\tilde{u}_{\parallel}(q_T) = (c_0 + c_1 q_T) \left(1 + \text{erf}(\alpha q_T^\beta)\right) \quad (7)$$

205 This step is only needed to check that amplitude of $\langle u_{\parallel} - \tilde{u}_{\parallel}(q_T) \rangle(\phi)$ is consistent with the
 206 amplitude of $\langle u_{\perp} \rangle(\phi)$ variation while the phase difference should be $\pi/2$.

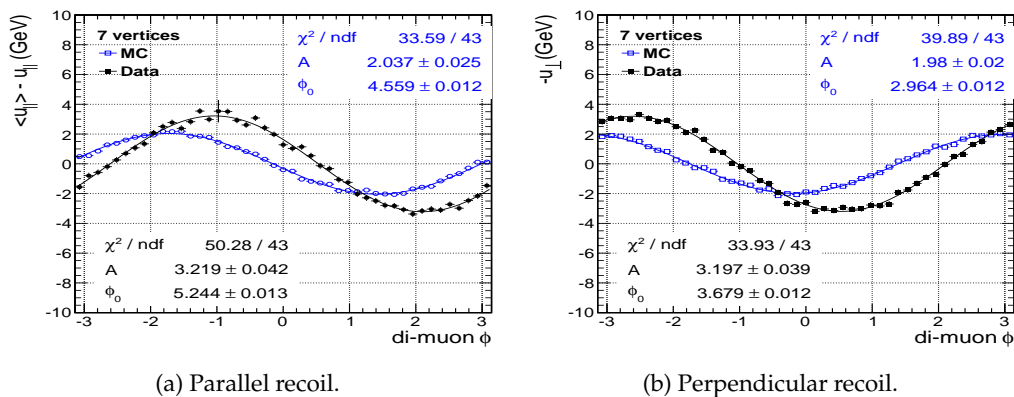
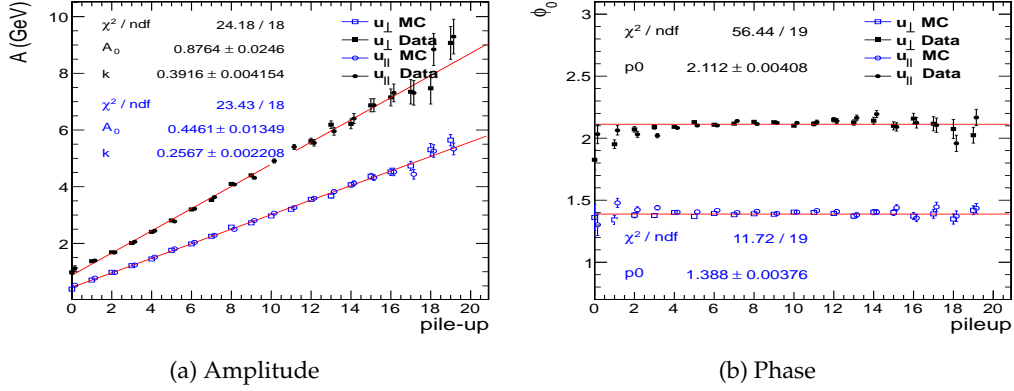


Figure 11: Parallel and perpendicular recoil as a function of boson ϕ for 7 reconstructed interaction vertices.

207 Figure 11 shows the profile of $\langle u_{\parallel} - \tilde{u}_{\parallel}(q_T) \rangle(\phi)$ and $\langle u_{\perp} \rangle(\phi)$ for 7 interaction vertices. Each
 208 such profile is fitted with $A_j(n) \cos(\phi - \phi_{0,j}(n))$, where n is the number of vertices, j denotes

Figure 12: Amplitude and phase of recoil ϕ modulation as a function of pile-up.

209 whether it's a perpendicular or parallel component. Then, on figure 12, we fit the amplitude
 210 of perpendicular recoil as a linear function of pile-up and the phase ($\phi_{0,\perp} - \pi/2$ for parallel
 211 component, $\phi_{0,\parallel} - \pi$ for perpendicular component) with constant function. The fit is only
 212 performed on perpendicular component. The parallel components are overlaid to check the
 213 consistency. So, to remove the ϕ modulation from E_T^{miss} , we add a 2d-vector to E_T^{miss} , whose
 214 direction is independent of (but different in data and MC) and the amplitude is a linear function
 215 of pile-up:

$$\vec{E}_X = \vec{E}_X + (A_0 + kn_{pu}) \cos(\phi_0) \quad (8)$$

$$\vec{E}_Y = \vec{E}_Y + (A_0 + kn_{pu}) \sin(\phi_0) \quad (9)$$

216 Note, this correction is independent of recoil axes and will be used in all MC samples and data.

217 6.2.3 Measure average parallel recoil

After having corrected E_T^{miss} for muon scale and ϕ modulation, we derive the average recoil as
 a function of boson q_T in 4 bins of leading jet $|\eta|$: [0.0-1.2], [1.2-2.4], [2.4-3.0], [3.0-5.0]. Jets are
 formed by clustering particle flow candidates, cleaned from particle flow muons that pass our
 quality criteria, with anti-kt algorithm with cone size of $R = 0.5$. Each average recoil profile is
 fitted with equation:

$$-\tilde{u}_{\parallel}(q_T) = (c_0 + c_1 q_T) \left(1 + \text{erf}(\alpha q_T^{\beta})\right) \quad (10)$$

218 As one can see from Figure 13, the difference between average recoil in data and MC is quite
 219 sensitive to η of the jet against which the boson is recoiling.

220 6.2.4 Measure recoil resolution

We measure the resolution of parallel and perpendicular recoil as a function of q_T for different
 number of reconstructed vertices. Figure 14 shows the distributions of u_{\perp} and $(u_{\parallel} - \tilde{u}_{\parallel}(q_T; \eta_{\text{jet}}))$
 for $10\text{GeV} < q_T < 12\text{GeV}$ and 7 interaction vertices. Each such distribution is fitted with the
 Gaussian. Figure 15 shows the σ of Gaussian from previous step, parametrized as a function of
 q_T with the following expression:

$$\sigma(q_T; n) = \sqrt{N_n^2 + S_n^2 q_T} \quad (11)$$

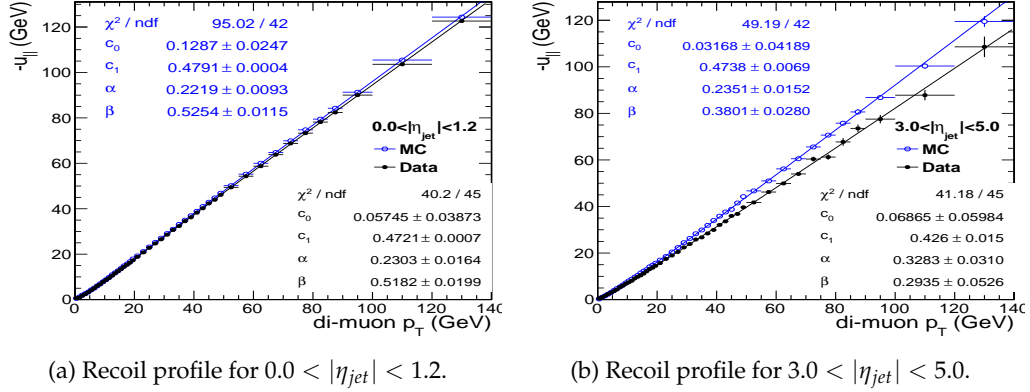
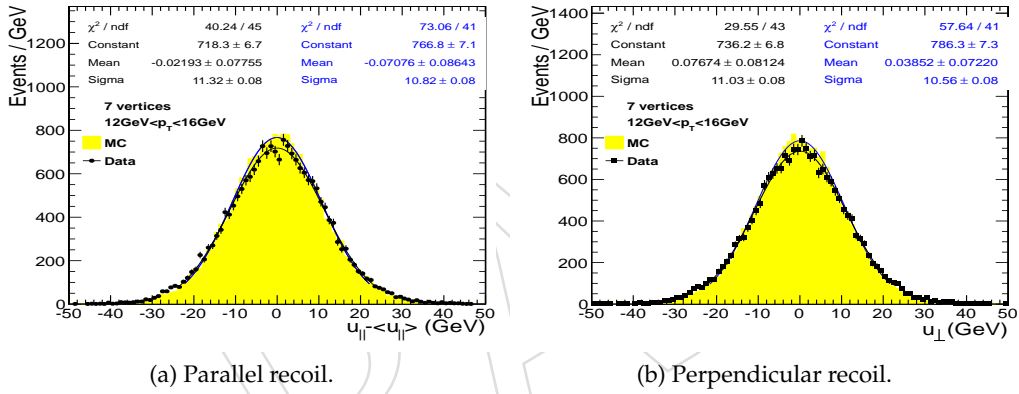
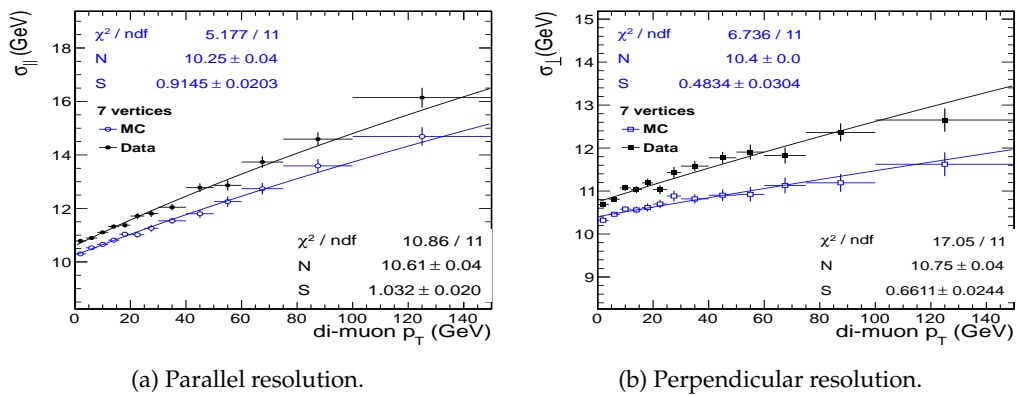
Figure 13: Amplitude and phase of recoil ϕ modulation as a function of pile-up.Figure 14: Parallel and perpendicular recoil variations for $10\text{GeV} < q_T < 12\text{GeV}$ and 7 interaction vertices.

Figure 15: Parallel and perpendicular recoil resolutions for 7 interaction vertices.

221 **6.3 Closure Test**

222 First we test the our MET tuning works in the Drell-Yan sample itself. Here we list the steps
 223 how the recoil correction is applied:

- 224 • correct E_T^{miss} for muon scale in both data and MC
- 225 • apply ϕ modulation corrections with Eq. 8 in both data and MC.
- shift the average and rescale the resolution of MC recoil components to match with data:

$$u_{\parallel} = \left(u_{\parallel} - \tilde{u}_{\parallel}^{\text{MC}} \right) \frac{\sigma_{\parallel}^{\text{DA}}}{\sigma_{\parallel}^{\text{MC}}} + \tilde{u}_{\parallel}^{\text{DA}} \quad (12)$$

$$u_{\perp} = u_{\perp} \frac{\sigma_{\perp}^{\text{DA}}}{\sigma_{\perp}^{\text{MC}}}, \quad (13)$$

226 where \tilde{u}_{\parallel} and $\sigma_{\parallel,\perp}$ are calculated with equations 10 and 11.

- 227 • recalculate MC E_T^{miss} with corrected recoil.

228 Figure 16 shows that recoil correction improves the agreement in E_T^{miss} between data and MC
 229 and removes $\Phi(E_T^{\text{miss}})$ modulation from both.

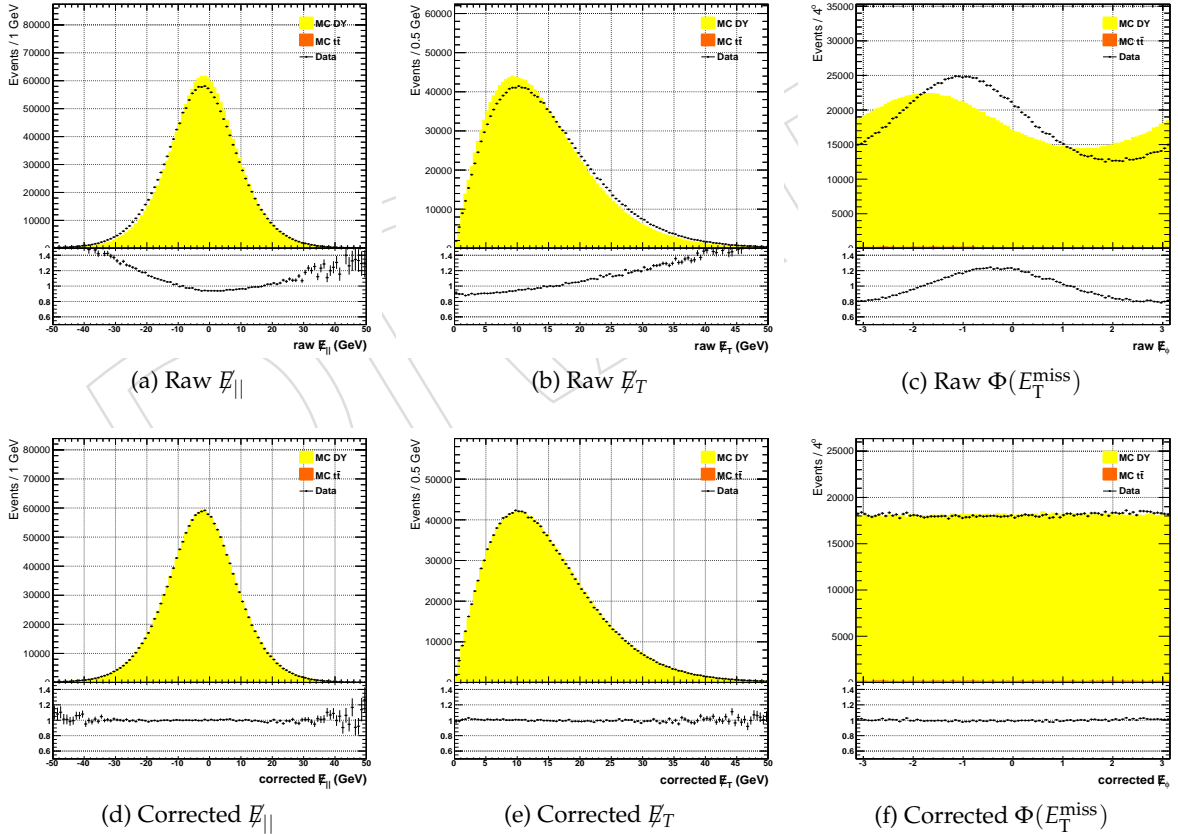


Figure 16: Uncorrected(top) and corrected (bottom) E_T^{miss} component distributions in Drell-Yan control sample.

230 6.4 Results

231 We fit the E_T^{miss} distribution in 11 muon pseudorapidity bins for each muon sign simultane-
232 ously, floating total number of W^+ (including overflow bin), total number of W^- and scale
233 factor of QCD events. Table 4 summarizes the results from each fit. The QCD scale factor
234 varies between 1.55 and 1.85 for different bins. The correlation between the QCD scale factor
235 and $N_{+,-}$ is about -22% . The χ^2 values show that the Monte-Carlo describes data pretty well.

236

237 (need to change correlation numbers)

238 Figure 17 shows the E_T^{miss} distributions for positive and negative muons after scaling signal
239 and QCD distributions according to fit results. The errors on the scale factors themselves are
240 not reflected in the data/MC ratio plots.

DRAFT

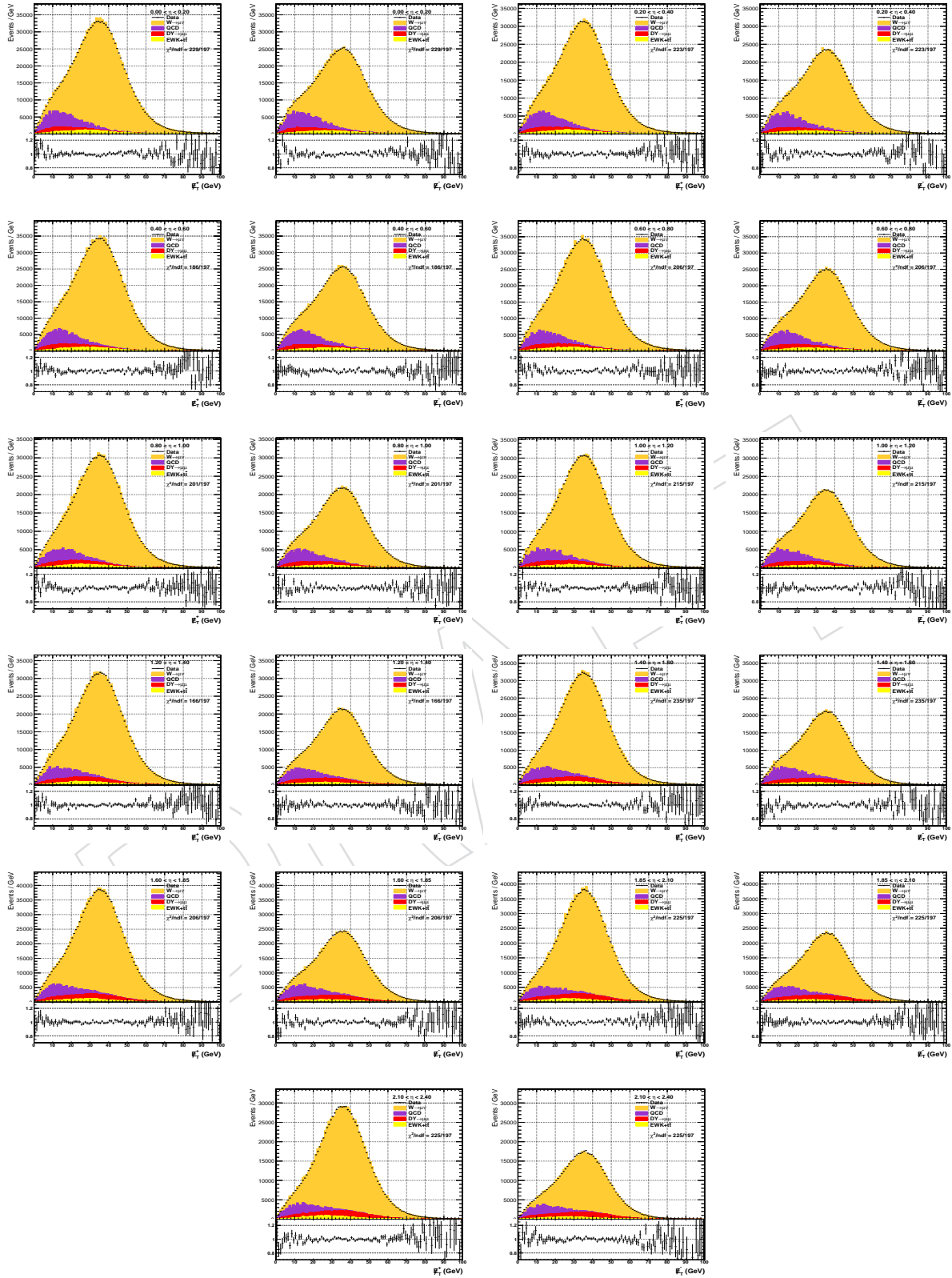


Figure 17: $E_T^{\text{miss}+}$ and $E_T^{\text{miss}-}$ distributions after fits in different bins.

7 Systematic Uncertainties

In this section we describe the asymmetry corrections and investigate possible sources of systematic errors that can affect EWK+ $t\bar{t}$ background normalization in each muon pseudorapidity bin and missing transverse momentum shapes. While performing event-by-event re-weighting for a systematic study we keep the overall (including all generated events) normalization of all Monte-carlo samples unchanged.

7.1 Muon efficiency

Efficiency uncertainty affects the asymmetry in two ways: first, if μ^+ and μ^- efficiencies are different then one should correct the measured asymmetry in selected events with the following equation,

$$A = A_0 - \frac{1 - A_0^2}{2} \left(\frac{\epsilon^+}{\epsilon^-} - 1 \right). \quad (14)$$

to get the true asymmetry before muon selection. Second, the muon efficiency also affects the background normalization. To estimate the systematic uncertainty we smear HLT and offline efficiency values in data and MC within their errors 400 times. In each pseudo experiment we use current efficiency values to scale MC EWK background normalization to data and measure raw asymmetry and correct it with the current ϵ^+/ϵ^- . We calculate the average efficiency in a given η bin as $\epsilon(\eta) = \Sigma f_{p_T} \epsilon(\eta, p_T)$, where f_k is the muon transverse momentum distribution in W events at generated level.

At the end we take the RMS of the result asymmetry distribution as the systematic error due to the efficiency. Figure 19c shows the measured asymmetry distribution in [1.85-2.10] pseudorapidity bin. Since the efficiencies are measured in the same η bins, there is no bin-to-bin correlation of asymmetry errors.

7.2 Integrated luminosity

Our current analysis data corresponds to total integrated luminosity of 2.26 fb^{-1} . It was calculated using Pixel detector based script and for runs and luminosity sections for which all CMS sub-detectors were declared as good ("Golden" json file). We use the integrated luminosity to normalize the EWK and $t\bar{t}$ samples. To estimate the systematic errors on asymmetry due to luminosity uncertainty, we vary it by $\pm 2.2\%$, and re-normalize all MC samples and redo the fits. We take the maximum deviation from the default value as the systematic uncertainty.

One should note that the varying luminosity changes the normalizations in all muon pseudorapidity bins coherently, such that bin-to-bin correlations of measured asymmetries are +100%.

7.3 Pile-Up

The pile-up affects the missing transverse energy shapes. To estimate the effect of mis-modeling the pile-up in the simulation, we vary the minimum bias cross-section by $\pm 5\%$ and re-generate pile-up re-weighting histograms and redo the fits.

Pile-up also affects E_T^{miss} shapes in all muon pseudorapidity bins coherently and the magnitude of correlation is again 100%. However since it's not a-priori obvious which way the asymmetry in a given bin will change as one increases the pile-up (it depends on how far and in which direction default resolutions of MC $E_T^{\text{miss}+}$ and $E_T^{\text{miss}-}$ are from data) the sign of bin-to-bin correlations can be both, positive and negative.

277 **7.4 PDF**

278 To evaluate the systematic errors due to PDF's we follow PDF4LHC recommendation, using
 279 CT10, NNPDF2.1 and MSTW2008nlo68cl PDF sets. We re-weight all events in all Monte-Carlo
 280 samples letting the overall normalization change. This way we cover both the uncertainty on
 281 the total cross-sections as well as the muon pseudorapidity shapes in EWK samples. While the
 282 main effect of PDF variation is that it changes the background normalization in each pseudo-
 283 rapidity bin, it also slightly affects the missing transverse momentum shape.

284 To estimate the systematic uncertainty for CT10 and MSTW sets, we use asymmetric master
 285 equations from [reference]. For CT10 we scale the 90%CL uncertainty to 68%CL one by the
 286 factor of 1.64485. For NNPDF set we take the RMS as the systematic error.

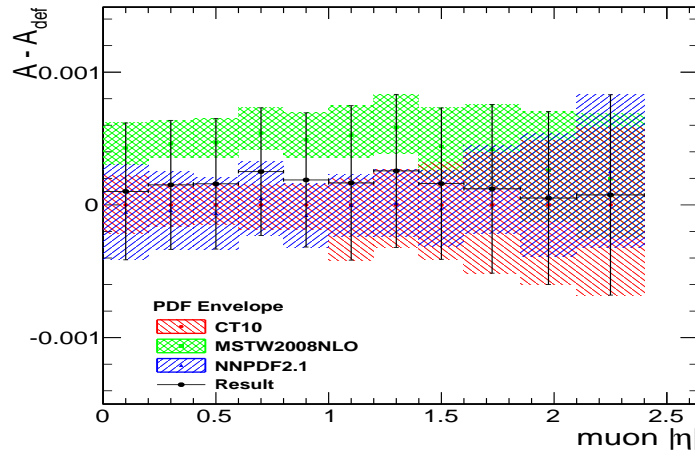


Figure 18: Systematic error bands for three different PDF sets.

287 Figure 18 shows the deviation from the default asymmetry value (which corresponds to central
 288 CT10 member) for three different PDF-sets vs the muon pseudorapidity. We take the middle
 289 point of the corresponding envelope as new central value for the asymmetry and half-width
 290 as a PDF systematic error, as indicated by black histogram (clearly MSTW biases the measured
 291 asymmetry and we will see at the end we can rule it out for the central bins, so I think I will
 292 take Hera PDF instead of MSTW for systematic evaluation).

293 To estimate bin to bin correlations, we use CT10 error set. For each of 26 parameter set varia-
 294 tions x_p and x_m :

- 295 • take the maximum deviation from default asymmetry value as uncertainty: $dA^i =$
 296 $maximum(|A_p^i - A_0^i|, |A_m^i - A_0^i|)$
- 297 • bin-to-bin correlation: $\rho^{i,j} = sign((A_p^i - A_m^i)(A_p^j - A_m^j))$

298 And add up covariance matrices. Table 5 shows the PDF correlation matrix. One can see that
 299 while varying PDF parameters, normalization in central and high eta bins change in opposite
 300 directions resulting in negative correlations between asymmetry values.

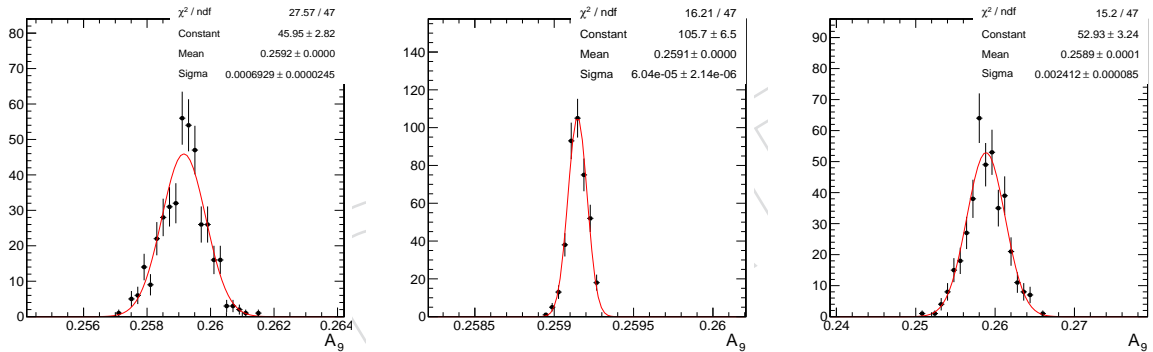
7.5 Muon momentum scale

The muon momentum scale correction affects data and Monte-Carlo yields and missing transverse momentum shape. To estimate the systematic error we smear muon $1/p_T$ correction parameters in each $\eta - \phi$ bin and global factor correction parameters within their errors 100 times, and each time we redo event selection and fitting steps.

Figure 19a shows the measured asymmetry distribution in $[1.85-2.10]$ pseudorapidity corresponding to 400 muon scale parameter set variations. We take the RMS of the measured asymmetry distribution in each muon pseudorapidity bin as systematic uncertainty and calculate bin-to-bin correlations.

7.6 Recoil correction

The recoil correction changes the missing transverse momentum shapes of all Monte-Carlo samples. To calculate the systematic errors we smear the recoil response and resolution parameters within their uncertainties, taking into account the correlations between them. Figure 19b shows the measured asymmetry distribution in $[1.85-2.10]$ pseudorapidity corresponding to 400 recoil parameter set variations. We take the RMS of the measured asymmetry distribution in each muon pseudorapidity bin as systematic uncertainty and calculate bin-to-bin correlations.



(a) Asymmetry distributions with smeared scale parameters. (b) Asymmetry distribution with smeared recoil parameters. (c) Asymmetry distribution with smeared muon efficiencies.

Figure 19: Asymmetry distributions with smeared muon momentum scale (a), recoil (b) and muon efficiencies (c) in $1.85 < |\eta| < 2.1$ bin.

7.7 $W p_T$ re-weighting

To improve the agreement between data and Monte-Carlo, we apply boson p_T re-weighting. The weight factors are measured by comparing $Z p_T$ distribution in data and Monte-Carlo. So we assume that the correction factors from Powheg to data in Z and W events are the same. To estimate the systematic errors due to this assumption we compare the $W/Z p_T$ ratio in Powheg Monte-Carlo to Madgraph.

Figure 20 shows W and Z generated q_T distributions in Powheg and Madgraph Monte-Carlos samples and ratio of $W q_T$ distributions in Powheg and Madgraph. The points on the left plot show the Powheg $W q_T$ distribution corrected with Madgraph/Powheg $Z q_T$ ratio. On the right plot, we fit the double-ratio distribution with the rational function with second order polynomials in numerator and denominator, which approaches unity at infinity. We use this

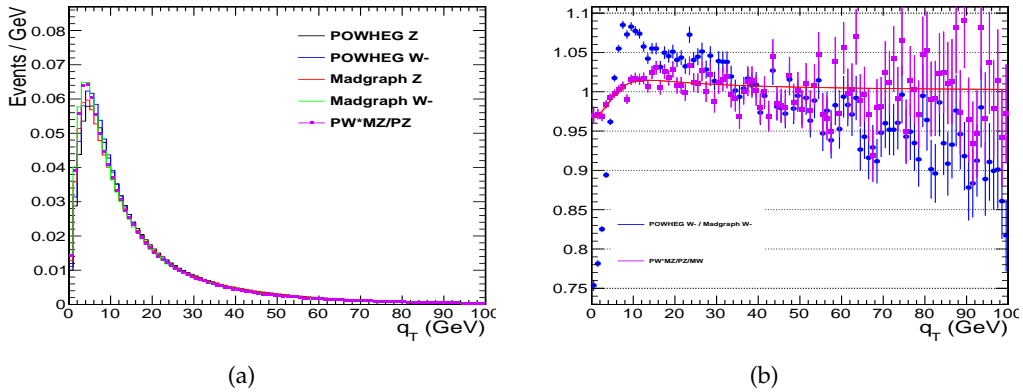


Figure 20: W and Z q_T distributions (a) and their ratios (b) in Madgraph and Powheg.

330 function and inverse of it to re-weight our W Monte Carlo samples event-by-event to study the
 331 systematic uncertainty associated with the assumption that the correction factors in W and Z
 332 events are the same. We take the maximum deviation of the measured asymmetries in these
 333 two cases from the default value as the systematic error.

334 7.8 QCD MET shape

335 By default we apply to QCD monte-carlo sample all MET corrections. In this section we look at
 336 how these corrections work in QCD control region. We select QCD control sample by requiring
 337 the isolated muon HLT to fail while at the same time non-isolated (prescaled) muon trigger to
 338 pass. We also invert the offline tracker isolation.

339 Figure 21 shows the MET distributions in QCD control region without (top) and with (bottom)
 340 corrections applied. To estimate the systematics associated with QCD MET shape, we remove
 341 the recoil correction part from QCD MC, re-do the fits and take the difference in result asym-
 342 metry as systematic error.

343 7.9 QCD +/-

344 By default we fix the QCD scale factor to be the same for μ^+ and μ^- fits. To estimate the
 345 systematic error associated with this assumption we let them float separately and take the
 346 difference between the result asymmetries and the default values as systematic uncertainty.

347 8 Results

348 First we present the result of the analysis performed in 22 muon pseudorapidity bins instead
 349 of 11, i.e. positive and negative η sides separately. Figure 22 shows the measured asymmetry
 350 distribution in positive (red square) vs. negative (blue circles) η sides. Error bars only include
 351 statistical errors on left-hand-side plots and statistical and efficiency uncertainties on right-
 352 hand-side ones. One can see that the asymmetry values are consistent within the errors once
 353 the efficiency and muon momentum scale corrections are applied.

354 In order to reduce the statistical errors, the final asymmetry values are measured in 11 $|\eta|$ bins,
 355 with positive and negative sides merged.

356 We also compare our measurement with ones performed in electron decay channel. Due to the
 357 trigger constraint the asymmetry in electron channel was measured with $p_T > 35$ GeV cut on

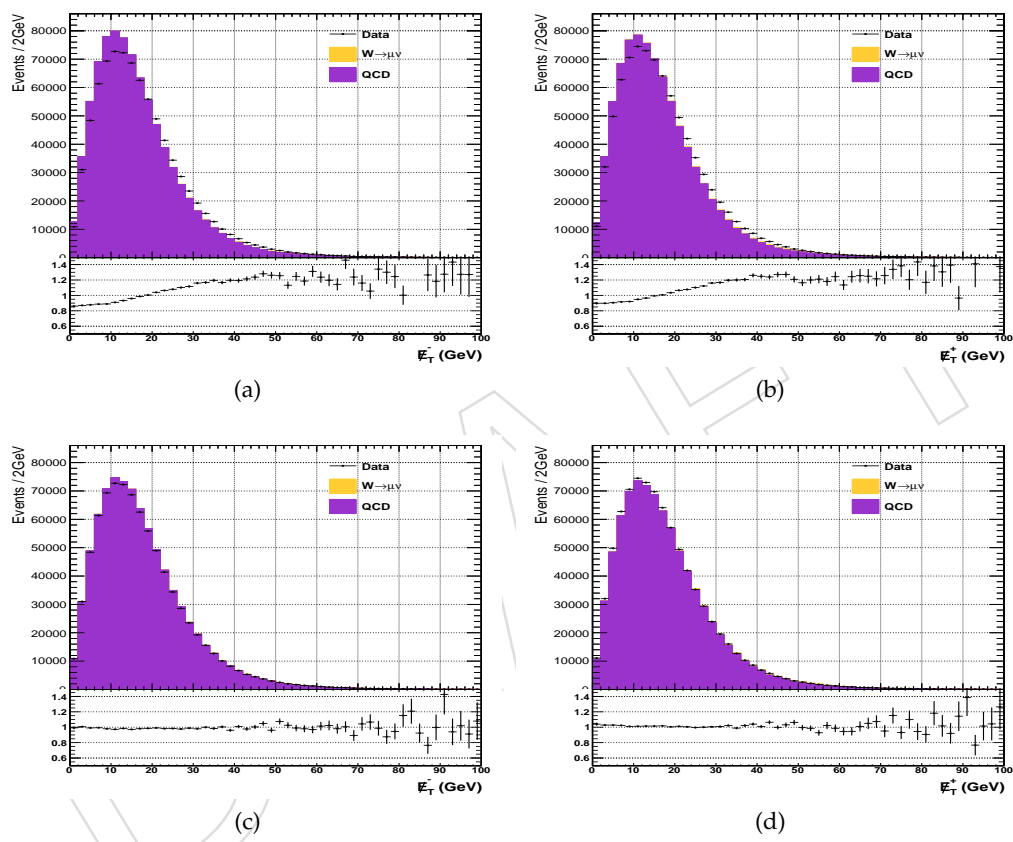
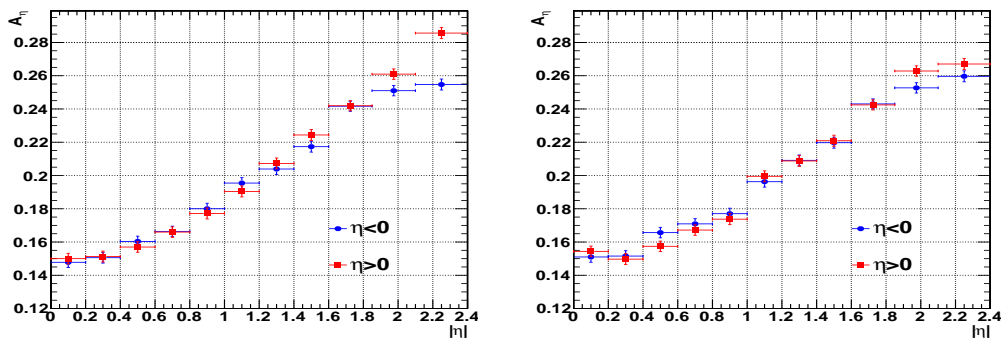
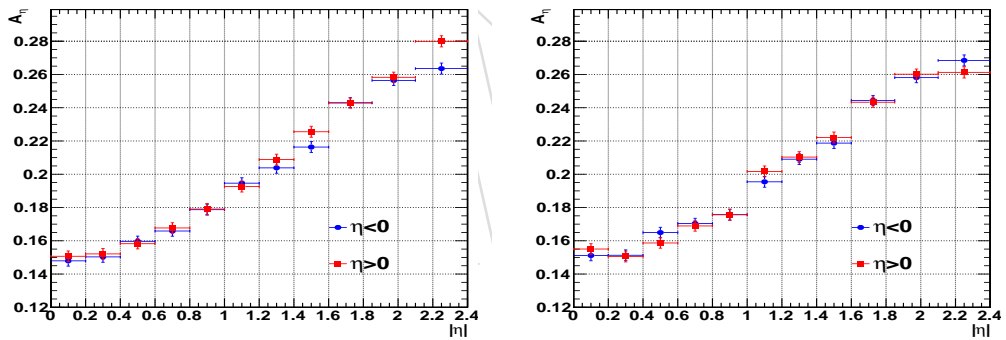


Figure 21: MET distributions with and without corrections.



(a) Without momentum scale and efficiency corrections. (b) Without momentum scale and with efficiency corrections.



(c) With momentum scale and without efficiency corrections. (d) With momentum scale and efficiency corrections.

Figure 22: Asymmetries in positive and negative η bins with and without muon scale and efficiency corrections.

358 the signal electron. Thus we also increase the threshold on the muon transverse momentum to
 359 the same value and repeat the analysis. Figure 23 shows good agreement between electron and
 360 muon results.

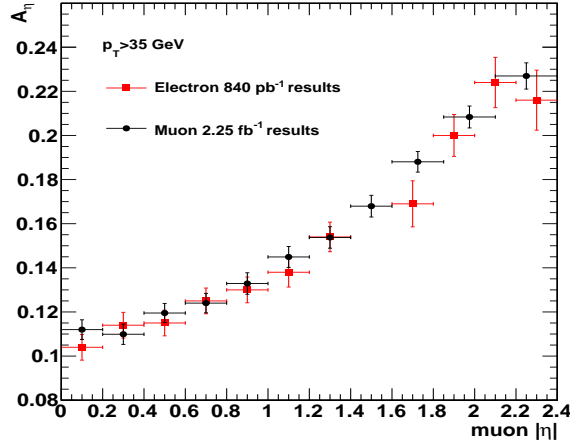
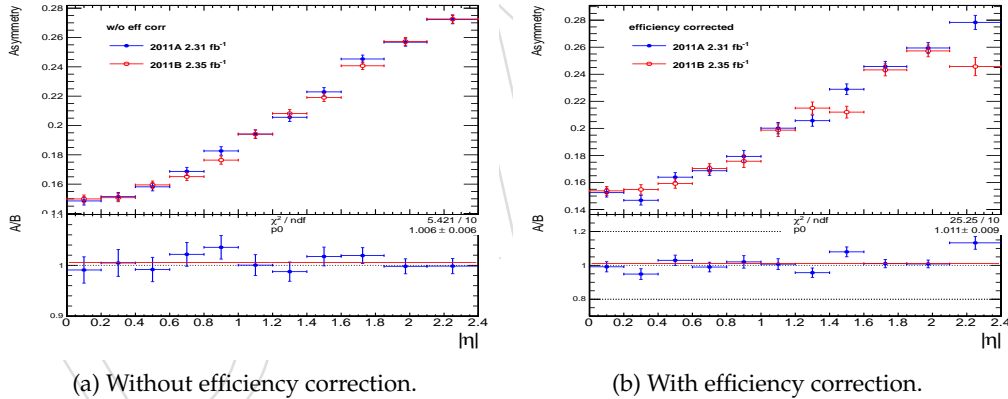


Figure 23: Muon vs electron asymmetry results for $p_T > 35\text{GeV}$].

361 We also measure separately the asymmetry in 2011A and 2011B data. Figure 24 shows the com-
 362 parison of measured asymmetries in 2011A vs 2011B without(left) and with(right) efficiency
 363 correction applied.



(a) Without efficiency correction.

(b) With efficiency correction.

Figure 24: Asymmetry in 2011A vs 2011B.

364 Table 6 shows the final result of asymmetry measurement in 11 muon pseudorapidity bins
 365 and breakdown of systematic errors. Current uncertainties in central bins are dominated by
 366 the statistical error from Monte-Carlo samples. The largest systematic contribution is due to
 367 $\epsilon^{data} / \epsilon^{mc}$ error, which is also of statistical nature and is driven by the limited Drell-Yan data
 368 sample.

369 Table ?? shows the correlation matrix of systematic uncertainties. Bin to bin correlations, as
 370 one can see from the table is rather small, since the dominant systematic uncertainty, $\epsilon^{data} / \epsilon^{mc}$,
 371 contributes independently in different $|\eta|$ bins. The remaining small correlations is mainly
 372 due-to the PDF uncertainties.

374 Figure 25 shows the comparison of measured asymmetry values with three different PDF models:
 375 CT10, NNPDF2.1 and MSTW2008. Data error bars include systematic and statistical errors
 376 added in quadrature. The theory bands for each PDF set was calculated FEWZ package for
 377 NLO with 68%CL. The first 10 bins are not corrected for efficiency while the last bin is cor-
 378 rected for the ϵ^+/ϵ^- .

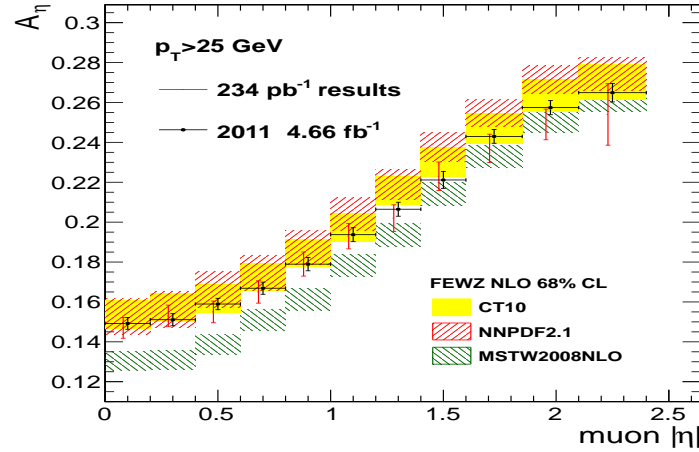


Figure 25: Comparison of measured asymmetry values with different PDF model predictions.

379 One can see that the measured asymmetry is in good agreement with CT10 and NNPDF predic-
 380 tions and when used in the global fits it can significantly reduce their parameter uncertainties.
 381 MSTW prediction is in significant disagreement with our measurement of asymmetry in central
 382 pseudorapidity bins.

383 9 Summary

384 References

- 385 [1] CMS Collaboration, “Measurements of inclusive W and Z cross sections in pp collisions
 386 at $\sqrt{s} = 7$ TeV”, *JHEP* **2** (2011) 2–40, doi:10.1007/JHEP01(2011)080,
 387 arXiv:hep-ph/10122466.
- 388 [2] A. D. Martin et al., “Parton distributions for the LHC”, *Eur. Phys. J.* **C63** (2009) 189–285,
 389 doi:10.1140/epjc/s10052-009-1072-5, arXiv:0901.0002.
- 390 [3] H.-L. Lai et al., “New parton distributions for collider physics”, *Phys. Rev.* **D82** (2010)
 391 074024, doi:10.1103/PhysRevD.82.074024, arXiv:1007.2241.
- 392 [4] J. D. Björken and E. A. Paschos, “Inelastic electron proton and gamma proton scattering,
 393 and the structure of the nucleon”, *Phys. Rev.* **185** (1969) 1975–1982,
 394 doi:10.1103/PhysRev.185.1975.
- 395 [5] CDF Collaboration, “Direct measurement of the W production charge asymmetry in $p\bar{p}$
 396 Collisions at $\sqrt{s} = 1.96$ TeV”, *Phys. Rev. Lett.* **102** (2009) 181801,
 397 doi:10.1103/PhysRevLett.102.181801, arXiv:0901.2169.
- 398 [6] D0 Collaboration, “Measurement of the electron charge asymmetry in
 399 $p\bar{p} \rightarrow W + X \rightarrow e\nu + X$ events at $\sqrt{s} = 1.96$ TeV”, *Phys. Rev. Lett.* **101** (2008) 211801,
 400 doi:10.1103/PhysRevLett.101.211801, arXiv:0807.3367.

- 401 [7] ATLAS Collaboration, "Measurement of the Muon Charge Asymmetry from W Bosons
402 Produced in pp Collisions at $\sqrt{s} = 7$ TeV with the ATLAS detector", *Phys.Lett. B* **701**
403 (2011) 31, doi:10.1016/j.physletb.2011.05.024, arXiv:1103.2929v1.
- 404 [8] CMS Collaboration, "Measurement of the lepton charge asymmetry in inclusive W
405 production in pp collisions at $\sqrt{s} = 7$ TeV", *JHEP* **04** (2011) 050,
406 doi:10.1007/JHEP04(2011)050, arXiv:1103.3470v1.
- 407 [9] LHCb Collaboration, "Inclusive W and Z production in the forward region at $\sqrt{s} = 7$
408 TeV", *JHEP* **06** (2012) 058, doi:10.1007/JHEP06(2012)058,
409 arXiv:1204.1620v3.
- 410 [10] CMS Collaboration, "Measurement of the muon charge asymmetry in inclusive W
411 production in pp collisions at $\sqrt{s} = 7$ TeV", CMS Physics Analysis Summary
412 CMS-PAS-EWK-11-005, (2011).
- 413 [11] CMS Collaboration, "Measurement of the electron charge asymmetry in inclusive W
414 production in pp collisions at $\sqrt{s} = 7$ TeV", CMS Physics Analysis Summary
415 CMS-PAS-SMP-12-001, (2012).
- 416 [12] P. Tan et al., "Muon Pseudorapidity and Charge Asymmetry in Inclusive
417 $pp \rightarrow W(\mu\nu) + X$ Production at $\sqrt{s} = 7$ TeV", CMS Analysis Note 2010/199, (2010).
- 418 [13] J. Bendavid et al., "Predictions on the lepton charge asymmetry and QED finite-state
419 radiation effect", CMS Analysis Note 2011/060, (2011).
- 420 [14] P. Tan et al., "The W Muon Charge Asymmetry in Inclusive $pp \rightarrow W(\mu\nu) + X$ Production
421 at $\sqrt{s} = 7$ TeV", CMS Analysis Note 2011/282, (2011).
- 422 [15] S. Frixione, P. Nason, and C. Oleari, "Matching NLO QCD computations with Parton
423 Shower simulations: the POWHEG method", *JHEP* **11** (2007) 070,
424 doi:10.1088/1126-6708/2007/11/070, arXiv:0709.2092.
- 425 [16] T. Sjöstrand, S. Mrenna, and P. Z. Skands, "PYTHIA 6.4 Physics and Manual", *JHEP* **05**
426 (2006) 026, doi:10.1088/1126-6708/2006/05/026, arXiv:hep-ph/0603175.
- 427 [17] J. Pumplin et al., "New generation of parton distributions with uncertainties from global
428 QCD analysis", *JHEP* **07** (2002) 012, arXiv:hep-ph/0201195.

429 .1 Introduction

430 Here, we describe briefly the muon efficiencies calculation methods and the parametr using
 431 the CMS Tag & Probe method and then to compare the values with cut & count method. The
 432 Tag and Probe tool is a well established data-driven approach to measure any user defined
 433 object efficiency from data at CMS.

434 The Tag & Probe method utilizes a known mass resonance (e.g. J/Ψ , Y and, Z) to select par-
 435 ticles of the desired type, and probe the efficiency of a particular selection criterion on those
 436 particles. In general the “tag” is an object that passes a set of very tight selection criteria de-
 437 signed to isolate the required particle type (muon μ , in this case). Tag muons are often referred
 438 to as golden muons, and the fake rate for passing tag selection criteria is very small. A generic
 439 set of the desired particle type (i.e. with potentially very loose selection criteria) known as
 440 “probe” is selected by pairing these objects with tags such that the invariant mass of the combi-
 441 nation is consistent with the mass of the resonance. The definition of the probe object depends
 442 on the specifics of the selection criterion being examined. These selections are described in
 443 the next subsection. Step-by-step instructions on the tag-and-probe package are described in
 444 “<https://twiki.cern.ch/twiki/bin/viewauth/CMS/ChargeAsymmetry2011>”.

445 A Cross Check of Muon Efficiencies

446 A.1 Muon Efficiencies and Comparisons

447 The tag muon selection is the same for each factor of the efficiency. The probe selection changes
 448 to reflect the efficiency being measured. The selection criteria for the tag, the passing probes
 449 and probes for each step are listed below.

450 The selection criteria for a tag muon is as follows and they are considered as “Tight” muon:

- 451 • reconstructed as both “GlobalMuon” and “TrackerMuon”,
- 452 • normalized global track fitting chisquared < 10 ,
- 453 • number of valid silicon track hits > 10 ,
- 454 • number of valid pixel track hits > 0 ,
- 455 • number of muon chamber hits > 0 ,
- 456 • track $|d_{xy}| < 2$ cm (with respect to the beam spot),
- 457 • track $d_z < 30$ cm,
- 458 • number of chambers with matched segments > 1 ,

459 and additional selections described as below,

- 460 • muon $|\eta| < 2.4$,
- 461 • matched to HLT_IsoMu24.
- 462 • track $p_T > 25$ GeV.

463 To study the tracking efficiency, a Standalone Muon candidate passing the all selection criteria
 464 as tag except $p_T > 15$ GeV was used as a probe.

465 To study the muon reconstruction and ID efficiency, a silicon track candidate passing the fol-
 466 lowing selection criteria was used as a probe,

- 467 • normalized track fitting chisquared < 10 ,

- 468 • track $|d_{xy}| < 2$ cm (with respect to the beam spot),
- 469 • track $d_z < 30$ cm,

470 We define the probe to be classified as a passing probe based on the “Tight” muon selection
471 criteria as outlined above for the Tag and $p_T > 15$ GeV.

472 To study the muon trigger (HLT_IsoMu24) efficiency, a good muon candidate passing the
473 “Tight” muon selection criteria for the tag muon except the $p_T > 15$ GeV was used as a probe.

474 A.1.1 Tracking Efficiency

475 The tracking efficiency is the probability that given a muon was generated in the event, it was
476 found as a muon silicon tracker track. In general, since the tracking efficiency in the silicon is
477 very high we can use all silicon tracker tracks as the probe sample to determine muon tracking
478 efficiency. The efficiency as a function of η is shown in Figure 26.

479 A.1.2 Global (Reconstruction) Efficiency

480 Reconstruction efficiency refers to the reconstruction of a muon track in the muon detectors. In
481 the language of CMSSW this is called a stand-alone muon track. The reconstruction efficiency
482 measures the probability that given a muon object track was found in the silicon trackers (mea-
483 sured above), a stand-alone muon track was also found. The efficiency as a function of η is
484 shown in Figure 27.

485 A.1.3 Identification (ID) Efficiency

486 The identification efficiency is the probability that given a muon tracker track and a stand-alone
487 muon track have been found (for the same muon) a global muon track is also reconstructed. A
488 probe is a muon that has a tracker track and a stand-alone track, while a passing-probe also has
489 a valid global muon fit. The efficiency as a function of η is shown in Figure 27.

490 A.1.4 Trigger Efficiency

491 The trigger efficiency is the unbiased efficiency that one of the Z muon daughters has fired
492 the trigger. To achieve an unbiased sample we require that the tag muon has fired the trigger.
493 Probe muons are all global muons with $p_T > 15.0 \text{ GeV}/c$ and passing probes are probes that
494 have also fired the selected trigger. The passing probes for the trigger efficiency measurement
495 are the same as the tags. The efficiency as a function of η is shown in Figure 28.

496 A.2 Results

497 In this subsection we present the results and compare the efficiencies with the corresponding
498 values obtained from cut & count method. The results are in Figures 26-28.

499 A.3 Conclusions

500 The muon efficiencies (global, tracking, identification, and trigger) in each pseudorapidity bin
501 and the p_T bins are measured using the $Z/\gamma^* \rightarrow \mu^+\mu^-$ data from 2011A data. They are com-
502 pared with the corresponding values from cut & count method and the results are comparable.

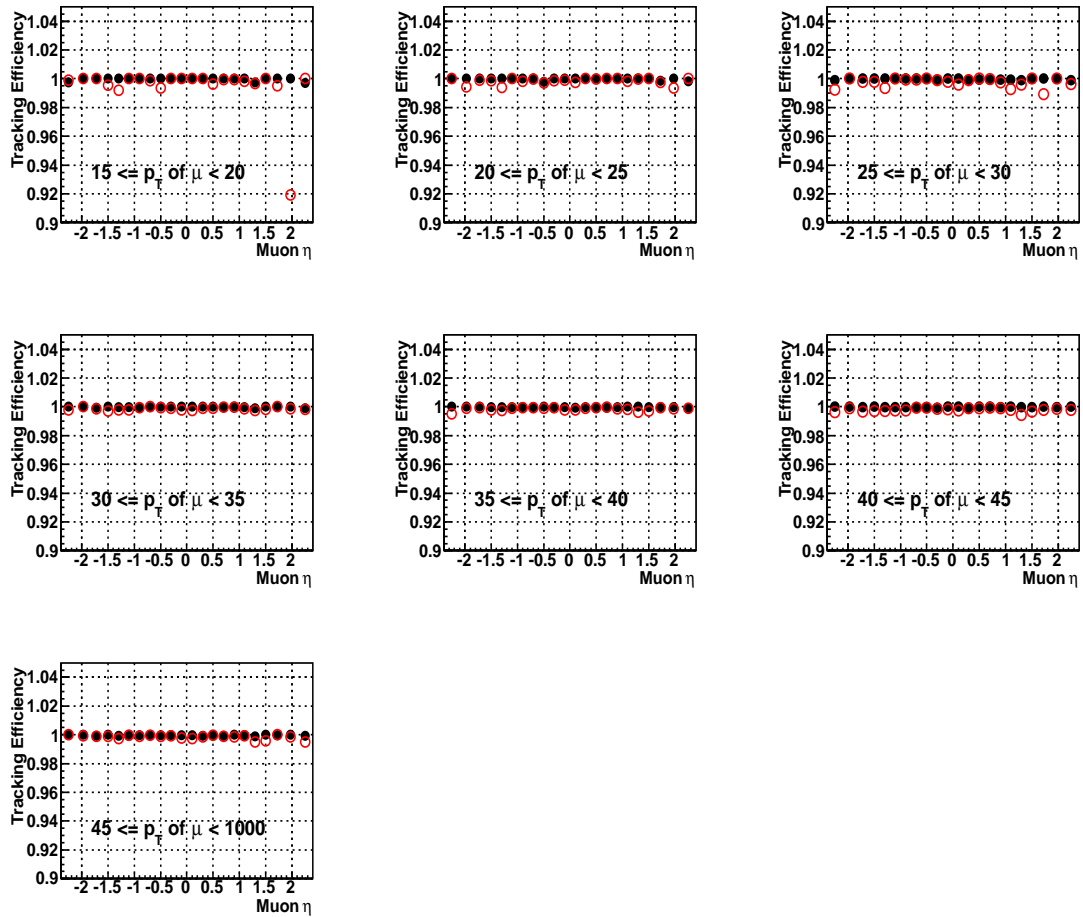


Figure 26: Comparison of **tracking** muon efficiencies as a function of η for all p_T bins. The open red circles and the black full circles show the efficiencies calculated from Tag& Probe method and cut & count method, respectively.

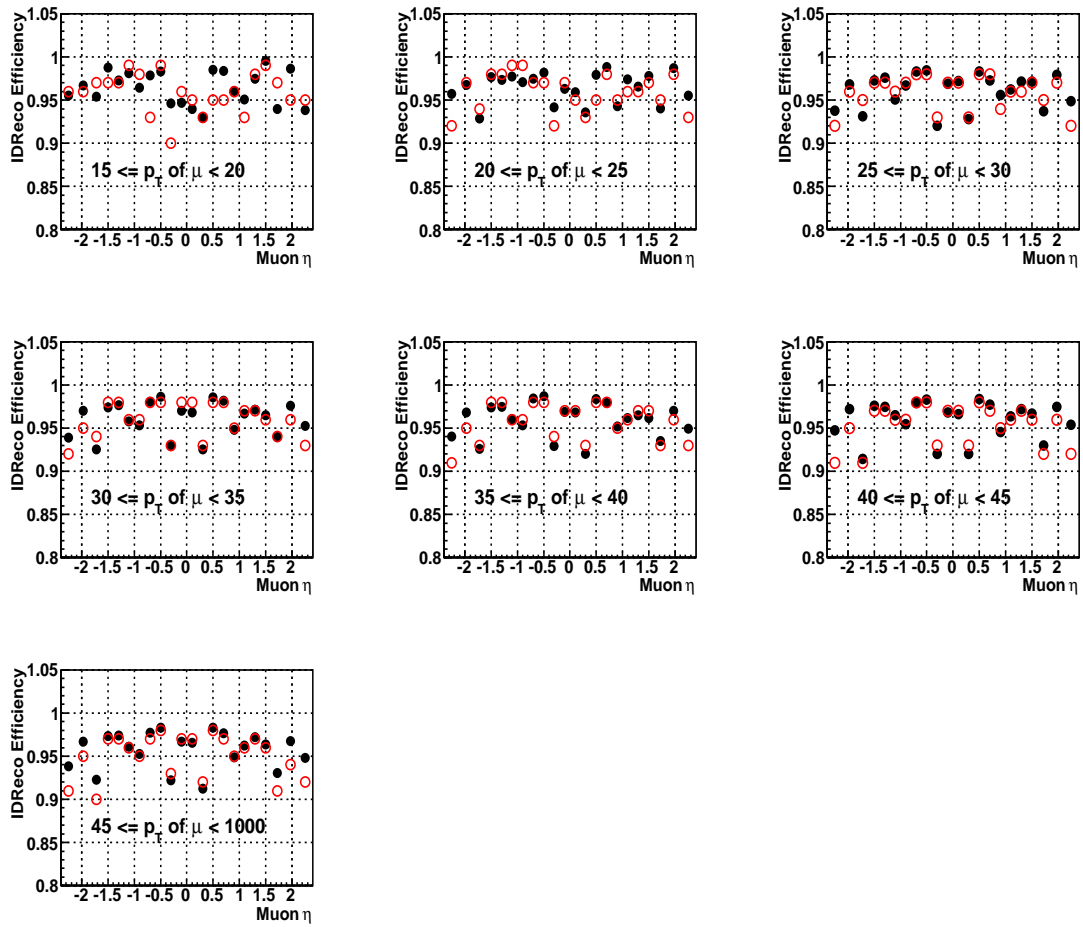


Figure 27: Comparison of muon $\epsilon_{reco+id}$ efficiencies as a function of η for all p_T bins. The open red circles and the black full circles show the efficiencies calculated from Tag& Probe method and cut & count method, respectively.

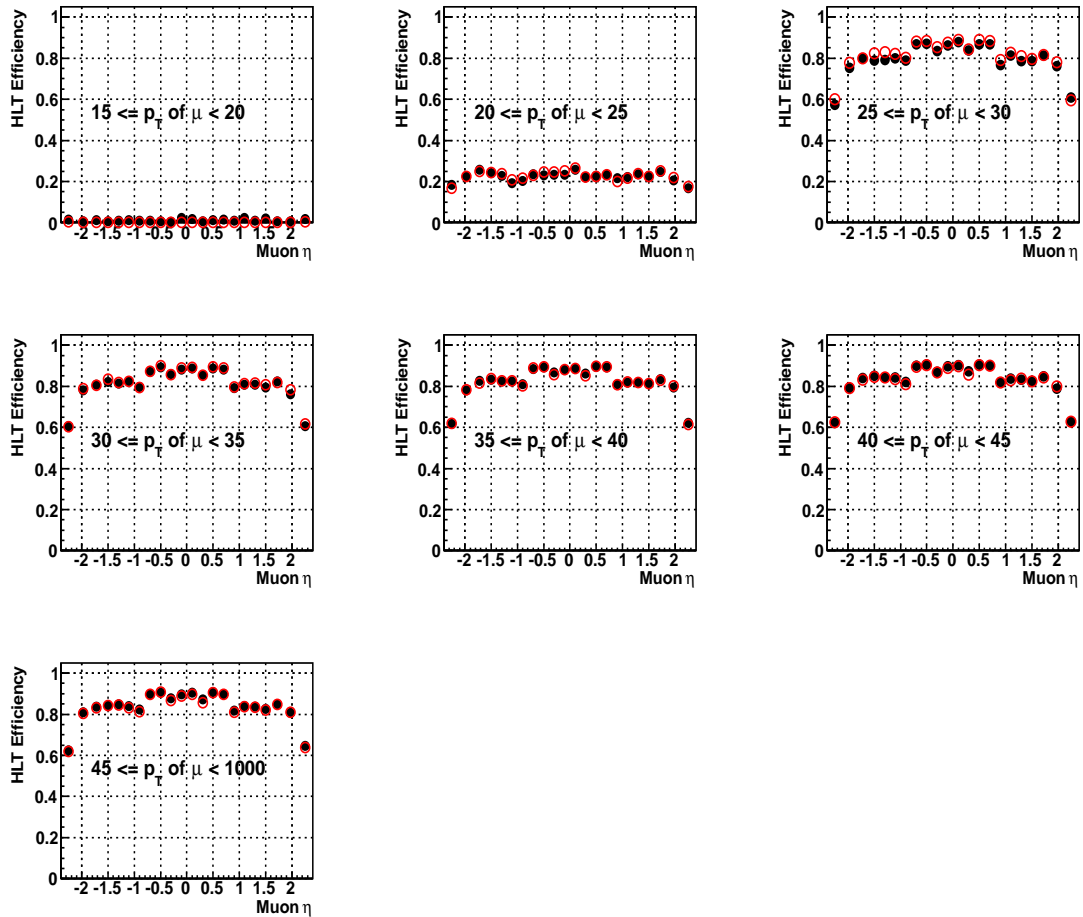


Figure 28: Comparison of muon **trigger** efficiencies as a function of η for all p_T bins. The open red circles and the black full circles show the efficiencies calculated from Tag& Probe method and cut & count method, respectively.

Table 4: Results from E_{miss} fits

η bin	N_+	N_-	a_{QCD}	$\rho_{N_+, a_{QCD}}$ (%)	$\rho_{N_-, a_{QCD}}$ (%)	ρ_{N_+, N_-} (%)	Asymmetry	$\chi^2(NDF = 197)$
0.00-0.20	1031871 \pm 3444	763897 \pm 2625	1.826 \pm 0.033	-21.67	-23.69	5.13	0.1492 \pm 0.0023	229
0.20-0.40	968542 \pm 3294	714287 \pm 2519	1.902 \pm 0.038	-22.91	-23.36	5.35	0.1511 \pm 0.0023	223
0.40-0.60	1063037 \pm 3473	771436 \pm 2640	1.844 \pm 0.036	-22.72	-22.44	5.10	0.1590 \pm 0.0022	186
0.60-0.80	1057149 \pm 3445	754774 \pm 2589	1.793 \pm 0.036	-22.78	-22.26	5.07	0.1669 \pm 0.0022	206
0.80-1.00	937752 \pm 3185	653078 \pm 2381	1.742 \pm 0.038	-23.47	-21.54	5.05	0.1789 \pm 0.0023	201
1.00-1.20	931074 \pm 3149	628881 \pm 2297	1.645 \pm 0.034	-22.01	-22.33	4.91	0.1937 \pm 0.0023	215
1.20-1.40	951148 \pm 3166	625585 \pm 2301	1.702 \pm 0.038	-23.04	-22.77	5.25	0.2065 \pm 0.0023	166
1.40-1.60	958918 \pm 3239	611605 \pm 2309	1.638 \pm 0.034	-22.32	-22.63	5.05	0.2211 \pm 0.0023	235
1.60-1.85	1136789 \pm 3521	692356 \pm 2474	1.633 \pm 0.031	-23.38	-22.00	5.14	0.2430 \pm 0.0021	206
1.85-2.10	1123056 \pm 3532	663225 \pm 2448	1.623 \pm 0.035	-22.20	-20.81	4.62	0.2574 \pm 0.0022	225
2.10-2.40	847612 \pm 2842	485363 \pm 1948	1.954 \pm 0.048	-22.05	-20.28	4.47	0.2718 \pm 0.0023	225

Table 5: PDF Correlation matrix

η bin	0.00-0.20	0.20-0.40	0.40-0.60	0.60-0.80	0.80-1.00	1.00-1.20	1.20-1.40	1.40-1.60	1.60-1.85	1.85-2.10	2.10-2.40
0.00-0.20	1.00	0.96	0.91	0.74	0.47	0.06	-0.22	-0.25	-0.37	-0.35	-0.38
0.20-0.40	0.96	1.00	0.92	0.74	0.54	0.12	-0.15	-0.16	-0.34	-0.34	-0.43
0.40-0.60	0.91	0.92	1.00	0.86	0.73	0.38	0.11	0.05	-0.11	-0.15	-0.32
0.60-0.80	0.74	0.74	0.86	1.00	0.85	0.62	0.35	0.30	0.18	0.10	-0.03
0.80-1.00	0.47	0.54	0.73	0.85	1.00	0.87	0.72	0.67	0.50	0.42	0.12
1.00-1.20	0.06	0.12	0.38	0.62	0.87	1.00	0.93	0.90	0.80	0.67	0.35
1.20-1.40	-0.22	-0.15	0.11	0.35	0.72	0.93	1.00	0.98	0.92	0.84	0.53
1.40-1.60	-0.25	-0.16	0.05	0.30	0.67	0.90	0.98	1.00	0.95	0.89	0.59
1.60-1.85	-0.37	-0.34	-0.15	0.18	0.50	0.80	0.92	0.95	1.00	0.95	0.73
1.85-2.10	-0.35	-0.34	-0.32	0.10	0.42	0.67	0.84	0.89	0.95	1.00	0.83
2.10-2.40	-0.38	-0.43	-0.32	-0.03	0.12	0.35	0.53	0.59	0.73	0.83	1.00

Table 6: Asymmetry results and uncertainties

$ \eta $ bin	0.00-0.20	0.20-0.40	0.40-0.60	0.60-0.80	0.80-1.00	1.00-1.20	1.20-1.40	1.40-1.60	1.60-1.85	1.85-2.10	2.10-2.40
Asymm Raw	0.14923	0.15109	0.15896	0.16688	0.17895	0.19372	0.20648	0.22114	0.24297	0.25742	0.27176
Eff corr	0.15301	0.15080	0.16182	0.16975	0.17574	0.19867	0.20984	0.22064	0.24391	0.25921	0.26491
Stat.	0.00225	0.00230	0.00222	0.00222	0.00232	0.00231	0.00229	0.00233	0.00215	0.00219	0.00235
St.inf:MC	0.00079	0.00081	0.00078	0.00078	0.00084	0.00084	0.00084	0.00084	0.00078	0.00079	0.00091
Lumi	0.00004	0.00003	0.00003	0.00007	0.00006	0.00012	0.00013	0.00017	0.00023	0.00031	0.00039
Pileup	0.00029	0.00012	0.00030	0.00008	0.00011	0.00031	0.00019	0.00019	0.00012	0.00018	0.00008
Recoil	0.00006	0.00007	0.00006	0.00007	0.00007	0.00006	0.00006	0.00007	0.00006	0.00006	0.00007
PDF	0.00052	0.00049	0.00049	0.00048	0.00051	0.00058	0.00058	0.00057	0.00064	0.00065	0.00075
Scale	0.00058	0.00061	0.00057	0.00060	0.00058	0.00062	0.00061	0.00065	0.00065	0.00069	0.00068
Eff	0.00146	0.00167	0.00144	0.00148	0.00219	0.00236	0.00220	0.00227	0.00233	0.00239	0.00367
W pt	0.00000	0.00000	0.00000	0.00000	0.00000	0.00000	0.00000	0.00000	0.00000	0.00000	0.00000
QCD+/-	0.00076	0.00070	0.00027	0.00112	0.00014	0.00036	0.00116	0.00263	0.00050	0.00030	0.00081
QCD shape	0.00044	0.00021	0.00064	0.00052	0.00061	0.00061	0.00037	0.00045	0.00077	0.00099	0.00079
Syst tot.	0.00189	0.00199	0.00179	0.00208	0.00241	0.00262	0.00266	0.00362	0.00268	0.00279	0.00399
Err tot.	0.00294	0.00304	0.00285	0.00304	0.00334	0.00350	0.00351	0.00430	0.00343	0.00355	0.00463